Physics

Physics Research Publications

Purdue University *Year* 2004

New measurements of Upsilon(1S) decays to charmonium final states

R. A. Briere, G. P. Chen, T. Ferguson, G. Tatishvili, H. Vogel, M. E. Watkins, N. E. Adam, J. P. Alexander, K. Berkelman, D. G. Cassel, J. E. Duboscq, K. M. Ecklund, R. Ehrlich, L. Fields, R. S. Galik, L. Gibbons, B. Gittelman, R. Gray, S. W. Gray, D. L. Hartill, B. K. Heltsley, D. Hertz, L. Hsu, C. D. Jones, J. Kandaswamy, D. L. Kreinick, V. E. Kuznetsov, H. Mahlke-Kruger, T. O. Meyer, P. U. E. Onyisi, J. R. Patterson, D. Peterson, J. Pivarski, D. Riley, J. L. Rosner, A. Ryd, A. J. Sadoff, H. Schwarthoff, M. R. Shepherd, W. M. Sun, J. G. Thayer, D. Urner, T. Wilksen, M. Weinberger, S. B. Athar, P. Avery, L. Breva-Newell, R. Patel, V. Potlia, H. Stoeck, J. Yelton, P. Rubin, B. I. Eisenstein, G. D. Gollin, I. Karliner, D. Kim, N. Lowrey, P. Naik, C. Sedlack, M. Selen, J. J. Thaler, J. Williams, J. Wiss, K. W. Edwards, D. Besson, K. Y. Gao, D. T. Gong, Y. Kubota, S. Z. Li, R. Poling, A. W. Scott, A. Smith, C. J. Stepaniak, J. Urheim, Z. Metreveli, K. K. Seth, A. Tomaradze, P. Zweber, J. Ernst, K. Arms, K. K. Gan, H. Severini, P. Skubic, D. M. Asner, S. A. Dytman, S. Mehrabyan, J. A. Mueller, V. Savinov, Z. Li, A. Lopez, H. Mendez, J. Ramirez, G. S. Huang, D. H. Miller, V. Pavlunin, B. Sanghi, E. I. Shibata, I. P. J. Shipsey, G. S. Adams, M. Chasse, J. P. Cummings, I. Danko, J. Napolitano, D. Cronin-Hennessy, C. S. Park, W. Park, J. B. Thayer, E. H. Thorndike, T. E. Coan, Y. S. Gao, F. Liu, R. Stroynowski, M. Artuso, C. Boulahouache, S. Blusk, J. Butt, E. Dambasuren, O. Dorjkhaidav, N. Menaa, R. Mountain, H. Muramatsu, R. Nandakumar, R. Redjimi, R. Sia, T. Skwarnicki, S. Stone, J. C. Wang, K. Zhang, A. H. Mahmood, S. E. Csorna, G. Bonvicini, D. Cinabro, M. Dubrovin, A. Bornheim, E. Lipeles, S. P. Pappas, and A. J. Weinstein

New measurements of $\Upsilon(1S)$ decays to charmonium final states

R. A. Briere, G. P. Chen, T. Ferguson, G. Tatishvili, H. Vogel, and M. E. Watkins
Carnegie Mellon University, Pittsburgh, Pennsylvania 15213, USA

N. E. Adam, J. P. Alexander, K. Berkelman, D. G. Cassel, J. E. Duboscq, K. M. Ecklund, R. Ehrlich, L. Fields, R. S. Galik, L. Gibbons, B. Gittelman, R. Gray, S. W. Gray, D. L. Hartill, B. K. Heltsley, D. Hertz, L. Hsu, C. D. Jones, J. Kandaswamy, D. L. Kreinick, V. E. Kuznetsov, H. Mahlke-Krüger, T. O. Meyer, P. U. E. Onyisi, J. R. Patterson, D. Peterson, J. Pivarski, D. Riley, J. L. Rosner,* A. Ryd, A. J. Sadoff, H. Schwarthoff, M. R. Shepherd, W. M. Sun, J. G. Thayer, D. Urner, T. Wilksen, and M. Weinberger
Cornell University, Ithaca, New York 14853, USA

S. B. Athar, P. Avery, L. Breva-Newell, R. Patel, V. Potlia, H. Stoeck, and J. Yelton
University of Florida, Gainesville, Florida 32611, USA

P. Rubin
George Mason University, Fairfax, Virginia 22030, USA

B. I. Eisenstein, G. D. Gollin, I. Karliner, D. Kim, N. Lowrey, P. Naik, C. Sedlack, M. Selen, J. J. Thaler, J. Williams, and J. Wiss
University of Illinois, Urbana-Champaign, Illinois 61801, USA

K. W. Edwards
Carleton University, Ottawa, Ontario, Canada K1S 5B6 and the Institute of Particle Physics, Canada

D. Besson
University of Kansas, Lawrence, Kansas 66045, USA

K. Y. Gao, D. T. Gong, Y. Kubota, S. Z. Li, R. Poling, A. W. Scott, A. Smith, C. J. Stepaniak, and J. Urheim
University of Minnesota, Minneapolis, Minnesota 55455, USA

Z. Metreveli, K. K. Seth, A. Tomaradze, and P. Zweber
Northwestern University, Evanston, Illinois 60208, USA

J. Ernst
State University of New York at Albany, Albany, New York 12222, USA

K. Arms and K. K. Gan
The Ohio State University, Columbus, Ohio 43210, USA

H. Severini and P. Skubic
University of Oklahoma, Norman, Oklahoma 73019, USA

D. M. Asner, S. A. Dytman, S. Mehrabyan, J. A. Mueller, and V. Savinov
University of Pittsburgh, Pittsburgh, Pennsylvania 15260, USA

Z. Li, A. Lopez, H. Mendez, and J. Ramirez
University of Puerto Rico, Mayaguez, Puerto Rico 00681

G. S. Huang, D. H. Miller, V. Pavlunin, B. Sanghi, E. I. Shibata, and I. P. J. Shipsey
Purdue University, West Lafayette, Indiana 47907, USA

G. S. Adams, M. Chasse, J. P. Cummings, I. Danko, and J. Napolitano
Rensselaer Polytechnic Institute, Troy, New York 12180

D. Cronin-Hennessy, C. S. Park, W. Park, J. B. Thayer, and E. H. Thorndike
University of Rochester, Rochester, New York 14627, USA

T. E. Coan, Y. S. Gao, F. Liu, and R. Stroynowski
Southern Methodist University, Dallas, Texas 75275, USA

M. Artuso, C. Boulahouache, S. Blusk, J. Butt, E. Dambasuren, O. Dorjkhaidav, N. Menaa, R. Mountain, H. Muramatsu, R. Nandakumar, R. Redjimi, R. Sia, T. Skwarnicki, S. Stone, J. C. Wang, and K. Zhang
Syracuse University, Syracuse, New York 13244, USA

A. H. Mahmood
University of Texas–Pan American, Edinburg, Texas 78539, USA

S. E. Csorna
Vanderbilt University, Nashville, Tennessee 37235, USA

G. Bonvicini, D. Cinabro, and M. Dubrovin
Wayne State University, Detroit, Michigan 48202, USA

A. Bornheim, E. Lipeles, S. P. Pappas, and A. J. Weinstein
California Institute of Technology, Pasadena, California 91125, USA

(CLEO Collaboration)

(Received 9 July 2004; published 5 October 2004)

Using data collected by the CLEO III detector at CESR, we report on measurements of $\Upsilon(1S)$ decays to charmonium final states. The data sample used for this analysis consists of 21.2×10^6 $\Upsilon(1S)$ decays, representing about 35 times more data than previous CLEO $\Upsilon(1S)$ data samples. We present substantially improved measurements of the branching fraction $\mathcal{B}(\Upsilon(1S) \to J/\psi + X)$ using $J/\psi \to \mu^+\mu^-$ and $J/\psi \to e^+e^-$ decays. The branching fractions for these two modes are averaged, thereby obtaining: $\mathcal{B}(\Upsilon(1S) \to J/\psi + X) = (6.4 \pm 0.4(\text{stat}) \pm 0.6(\text{syst})) \times 10^{-4}$. A greatly improved measurement of the J/ψ momentum distribution is presented and indicates a spectrum which is much softer than predicted by the color-octet model and somewhat softer than the color-singlet model. First measurements of the J/ψ polarization and production angle are also presented. In addition, we report on the first observation of $\Upsilon(1S) \to \psi(2S) + X$ and evidence for $\Upsilon(1S) \to \chi_{cJ} + X$. Their branching fractions are measured relative to $\mathcal{B}(\Upsilon(1S) \to J/\psi + X)$ and are found to be $\{[\mathcal{B}(\Upsilon(1S) \to \psi(2S) + X)]/[\mathcal{B}(\Upsilon(1S) \to J/\psi + X)]\} = 0.41 \pm 0.11(\text{stat}) \pm 0.08(\text{syst})$, $\{[\mathcal{B}(\Upsilon(1S) \to \chi_{c1} + X)]/[\mathcal{B}(\Upsilon(1S) \to J/\psi + X)]\} = 0.35 \pm 0.08(\text{stat}) \pm 0.06(\text{syst})$, $\{[\mathcal{B}(\Upsilon(1S) \to \chi_{c2} + X)]/[\mathcal{B}(\Upsilon(1S) \to J/\psi + X)]\} = 0.52 \pm 0.12(\text{stat}) \pm 0.09(\text{syst})$, and $\{[\mathcal{B}(\Upsilon(1S) \to \chi_{c0} + X)]/[\mathcal{B}(\Upsilon(1S) \to J/\psi + X)]\} < 7.4$ at 90% confidence level. The resulting feed-down contributions to J/ψ are $[24 \pm 6(\text{stat}) \pm 5(\text{syst})]\%$ for $\psi(2S)$, $[11 \pm 3(\text{stat}) \pm 2(\text{syst})]\%$ for χ_{c1}, $[10 \pm 2(\text{stat}) \pm 2(\text{syst})]\%$ for χ_{c2}, and $<8.2\%$ at 90% confidence level for χ_{c0}. These measurements (apart from χ_{c0}) are about a factor of 2 larger than expected based on the color-octet model.

DOI: 10.1103/PhysRevD.70.072001 PACS numbers: 13.25.Gv

I. INTRODUCTION

Charmonium has played a crucial role in the recent history of particle physics. It has been nearly 30 years since its discovery in both e^+e^- interactions [1] and in collisions of protons on a beryllium target [2]. Over the last two decades, the charmonium and bottomonium systems have served as a laboratory for testing QCD. In the weak sector, charmonium also serves as a critical tool in extracting Cabibbo-Kobayashi-Maskawa [3] phases in B-meson decays. However, even after 30 years of studying $c\bar{c}$ systems, we still lack a complete understanding of their production mechanisms in glue-rich environments.

About a decade ago, the CDF experiment reported production rates of charmonium in proton-antiproton collisions which exceeded the existing theoretical calculations by a factor of about 10 for J/ψ and about a factor of 50 for $\psi(2S)$ [4]. An explanation of this excess was given by the so-called *color-octet* mechanism [5], whereby a gluon fragments into a color-octet $3S_1$ $c\bar{c}$ pair, which then evolves nonperturbatively into a color singlet by emission of a soft gluon. The size of this nonperturbative matrix element is not predicted and was determined by a fit to the CDF data. Because of the glue-rich environment and the α_s^2 suppression of the

*On leave of absence from University of Chicago.

color-singlet process relative to the color-octet process, it was argued [5] that the latter contribution is likely to be important. While this model can explain the rate and momentum spectrum of J/ψ and $\psi(2S)$ production at the Tevatron it appears that it does not properly describe recent J/ψ polarization data from CDF [6]. Furthermore, when the same matrix elements determined at CDF are applied to photoproduction of J/ψ at HERA, the color-octet contribution is about a factor of 10 too large [7].

Over the last several years, the role of the color-octet mechanism in J/ψ production in e^+e^- collisions has been under theoretical study [8]. The dynamics of the color-octet processes are expected to give rise to significant differences in the J/ψ momentum spectrum and production angle as compared to color-singlet production. Recently, both *BABAR* [9] and Belle [10] have reported measurements of the cross section and the momentum spectra of J/ψ's in e^+e^- collisions on the $\Upsilon(4S)$ (B decays excluded) or just below the $\Upsilon(4S)$ (i.e., in the continuum). *BABAR* measures $\sigma(e^+e^- \to J/\psi + X) = (2.52 \pm 0.21 \pm 0.21)$ pb, whereas Belle measures a number which is 40% lower, $(1.47 \pm 0.10 \pm 0.13)$ pb (about 3 standard deviations below that of the *BABAR* result). The two experiments both observe similar shapes for the J/ψ momentum spectrum, which are softer than the predictions of the color-octet model [8] which predict a peaking of the J/ψ momentum spectrum near the kinematic end point. However, recent theoretical studies of the color-octet subprocesses, $e^+e^- \to J/\psi + g$ [11] and $e^+e^- \to J/\psi + gg$ [12], show that the perturbative expansion breaks down near the kinematic end point, and the authors appeal to soft-collinear effective theory (SCET) to systematically include the nonperturbative effects. In Ref. [11], it is shown that by using SCET the color-octet model predictions can be sufficiently softened and reasonably good agreement with $e^+e^- \to J/\psi + X$ data can be achieved, although the calculation is not completely predictive because it uses a shape function which is fit to the $e^+e^- \to J/\psi + X$ data [9,10]. Belle also reports on production of $\psi(2S)$ in e^+e^- collisions, with a measured ratio $\sigma(e^+e^- \to \psi(2S) + X)/\sigma(e^+e^- \to J/\psi_{\rm direct} + X) = 0.93 \pm 0.17^{+0.13}_{-0.15}$ [10]. That is, the production rates for J/ψ and $\psi(2S)$ in e^+e^- collisions are approximately equal. The color-singlet mechanism can yield the $\psi(2S)$ final state, but the expected ratio is $\leq 10\%$ [13]. Belle has extended their inclusive J/ψ analysis to search for associated charmed particles, and they find $\sigma(e^+e^- \to J/\psi c\bar{c})/\sigma(e^+e^- \to J/\psi + X) = 0.59^{+0.15}_{-0.13} \pm 0.12$ [14]. The color-octet contribution is expected to be at the level of 1% [15] of the inclusive rate. The disagreement here indicates that the production mechanisms of charmonium are not well understood, and more theoretical and experimental input is required.

Several theoretical papers [15,16] have suggested that the study of J/ψ production in $\Upsilon(1S)$ decays could provide an alternate probe of the charmonium system in that the $\Upsilon(1S)$ decay provides a glue-rich environment in which J/ψ mesons can be produced abundantly through the color-octet mechanism. The kinematics of such J/ψ's are expected to exhibit signatures distinct from other production mechanisms, such as a peak in the J/ψ momentum spectrum near the kinematic end point. The predicted branching fraction from color-octet processes is $\mathcal{B}(\Upsilon(1S) \to J/\psi + X) = 6.2 \times 10^{-4}$ [16], with approximately 10% feed-down expected from $\psi(2S)$ and another 10% from χ_{cJ} [17] (summed over all J). Color-singlet processes, such as $\Upsilon(1S) \to J/\psi + gg$ start at α_s^6, and are therefore suppressed relative to color-octet processes which enter at α_s^4. However, computations of the color-singlet process $\Upsilon(1S) \to J/\psi c\bar{c}g + X$ [13] indicate a sizable branching fraction of 5.9×10^{-4}, with about 10% coming from $\psi(2S)$ feed-down. The enhancement here arises because the nonperturbative color-singlet matrix element for $c\bar{c} \to J/\psi$ may be 210–360 times larger than the corresponding color-octet matrix element, which is enough to compensate for the perturbative suppression. Moreover, unlike the color-octet processes, this process inherently results in a soft J/ψ momentum spectrum because of the two additional charm quarks in the final state. As a result, the J/ψ momentum cannot exceed about 3.3 GeV/c in this process. Therefore, while the color-octet and color-singlet processes give similar predictions for total rate, their momentum distributions are significantly different. Figure 1 shows Feynman diagrams for (a) two of the more important color-octet processes and (b) the $\Upsilon(1S) \to J/\psi c\bar{c}g + X$ color-singlet diagram. It should be noted that color-singlet production would also be signaled by the presence of additional charmed particles (open charm) in association with the J/ψ. To capitalize on the small yield of J/ψ's in $\Upsilon(1S)$ decay, many D decay channels, both inclusive and exclusive, will need to be explored. We therefore relegate the search for open charm in association with J/ψ in $\Upsilon(1S)$ decay to a future report.

The process $\Upsilon(1S) \to J/\psi + X$ has been previously observed by CLEO [18], where the branching fraction was measured to be $(1.1 \pm 0.4 \pm 0.2) \times 10^{-3}$ based on ≈ 20 observed events. CLEO also reported a soft momentum spectrum for the J/ψ, albeit with limited statistical precision. The ARGUS Collaboration reported an upper limit of 0.68×10^{-3} [19] at 90% confidence level.

The CLEO Collaboration has collected large data samples on the $\Upsilon(nS)$ resonances and currently has the world's largest samples of $\Upsilon(1S)$, $\Upsilon(2S)$, and $\Upsilon(3S)$ decays. Consequently, CLEO is in a unique position to help clarify the roles of color-singlet and color-octet models in J/ψ production.

In this paper, we present vastly improved measurements of the rate, momentum spectrum, and angular distributions in $\Upsilon(1S) \to J/\psi + X$ decays. We also

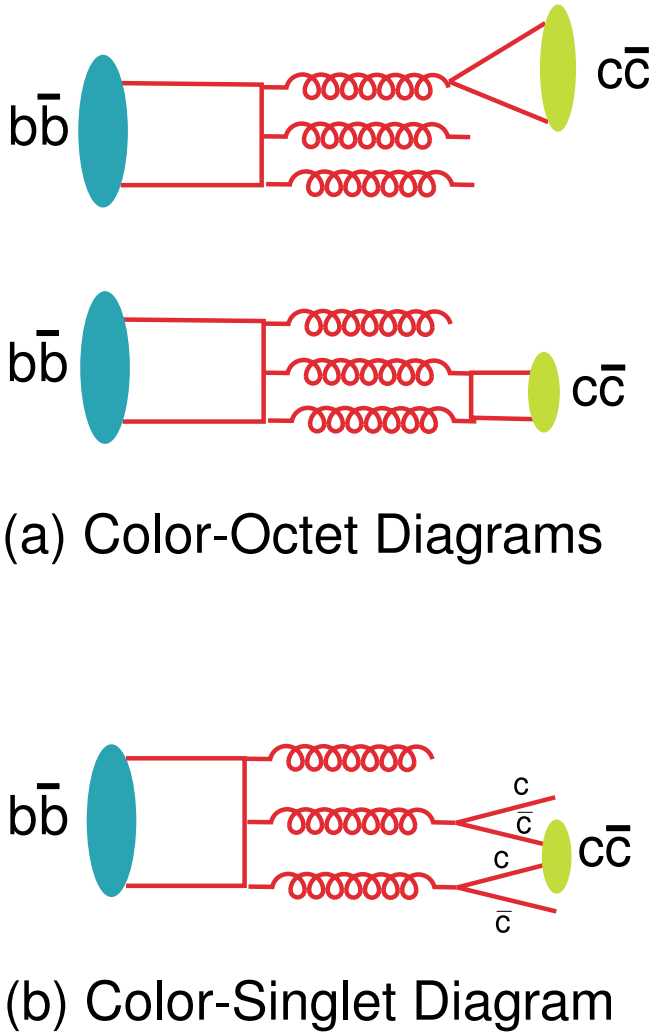

FIG. 1 (color online). Feynman diagrams for production of charmonium in $\Upsilon(1S)$ decays from (a) color-octet processes and (b) color singlet $\Upsilon(1S) \to J/\psi c\bar{c}g + X$. For the color-octet processes, the J/ψ is produced in a color octet and becomes a color singlet through emission of a soft gluon.

present first observations of the decays $\Upsilon(1S) \to \psi(2S) + X$ and evidence for $\Upsilon(1S) \to \chi_{c1,2} + X$. The paper is organized as follows. In Sec. II we discuss the data samples used, the J/ψ backgrounds, event selection, and J/ψ reconstruction. Section III details the measurement of the $\Upsilon(1S) \to J/\psi + X$ branching fraction and momentum spectrum in $\Upsilon(1S)$ decays. This section also includes a measurement of the cross section $\sigma(e^+e^- \to J/\psi + X)$ using data on and below the $\Upsilon(4S)$ resonance, which is used to estimate and subtract the continuum contribution at the $\Upsilon(1S)$. The section concludes with an examination of some event-level distributions. Section IV presents the measurement of the $\Upsilon(1S) \to \psi(2S) + X$ branching fraction. The report then discusses in Sec. V the measurement $\mathcal{B}(\Upsilon(1S) \to \chi_{cJ} + X)$. For each of these analyses, we present a cross-check by measuring the corresponding branching fraction in B-meson decay. Lastly, we discuss in Sec. VI the systematic uncertainties in each of these analyses, and the paper is concluded in Sec. VII.

II. DATA SAMPLES, BACKGROUNDS, EVENT SELECTION, AND J/ψ RECONSTRUCTION

The analysis presented here uses data collected using the CLEO III detector [20]. The primary data sample includes 1.2 fb^{-1} of data collected on the $\Upsilon(1S)$ and amounts to $(21.2 \pm 0.2) \times 10^6$ $\Upsilon(1S)$ decays. For background determinations and systematic checks, we also utilize 5.0 fb^{-1} of data on the $\Upsilon(4S)$ resonance (10.4×10^6 B-meson decays) and 2.3 fb^{-1} just below ($\approx$10.56 GeV) the $\Upsilon(4S)$ resonance. We also use the on-$\Upsilon(4S)$ data for cross-checks on charmonium yields in B-meson decays.

The backgrounds to $J/\psi \to l^+l^-$ on the $\Upsilon(1S)$ are (i) radiative Bhabha events, (ii) $\gamma\gamma$ fusion producing χ_{cJ} which subsequently produces $J/\psi\gamma$, (iii) radiative return processes such as $e^+e^- \to J/\psi\gamma$ or $e^+e^- \to \psi(2S)\gamma$, and (iv) continuum production ($e^+e^- \to J/\psi + X$). Various event selection requirements are targeted at reducing or eliminating these backgrounds. Radiative Bhabha events produce background in the J/ψ mass region when one of the hard leptons is combined with a soft lepton from the converted photon. Such events are suppressed by requiring that the invariant mass of either electron from the $J/\psi \to e^+e^-$ candidate with any other electron in the event has $M_{ee} > 100$ MeV/c^2. Events produced through $\gamma\gamma \to \chi_{cJ}$ fusion typically leave only two charged tracks in the CLEO III detector, and these events are therefore easily rejected by a requirement of at least three charged tracks. The radiative return backgrounds are suppressed through event selection criteria which take advantage of the special kinematics of these processes, namely, a low particle multiplicity coupled with either the detection of a high energy photon ($\approx$ 4 GeV) or large missing event momentum. Events are required to have their missing event momentum magnitude, $P_{\text{ev}} < 3.75$ GeV/c, or, if the number of charged tracks, $N_{\text{trk}} \leq 4$, we require $P_{\text{ev}} < 2.0$ GeV/c. When the high energy photon is detected (or an e^+e^- pair with invariant mass less than 100 MeV/c^2), the event is vetoed if $N_{\text{trk}} \leq 4$ and the (converted) photon has energy greater than 3.75 GeV. The remaining background from these three sources to the $\Upsilon(1S) \to J/\psi + X$ signal is negligible. However, because of the small signal in $\Upsilon(1S) \to \psi(2S) + X$, the remaining background cannot be neglected. This background is determined using the EVTGEN Monte Carlo (MC) followed by a GEANT-based detector simulation, and the resulting contribution is subtracted from the observed yields.

Continuum background is reduced by requiring that the second Fox-Wolfram moment [21] $R_2 < 0.6$. The remainder of this background is estimated using $\Upsilon(4S)$ data and is statistically subtracted from the observed $\Upsilon(1S)$ yields.

The estimate of this background is discussed in Secs. III B and III E.

Candidate J/ψ's are formed by pairing oppositely charged electron or muon candidates. These charged-track candidates are required to have momentum in the range from 0.1 to 5.3 GeV/c and have at least 50% of the maximum number of expected hits in the tracking system. We also require these tracks to be consistent with coming from the interaction point in three dimensions. Electron candidates are additionally required to have a shower profile which is consistent with expectations for an electron and an energy deposition in the calorimeter, E_e, which is compatible with its measured momentum, p_e, by requiring $0.85 < E_e/p_e < 1.15$. For these electron candidates, we correct for radiated photons by adding back the momentum of the highest energy photon which lies within a 5° cone of the initial particle direction. Muon candidates are formed using charged tracks which penetrate at least three hadronic interaction lengths of iron absorber in the muon chambers [20].

III. MEASUREMENTS OF $\Upsilon(1S) \rightarrow J/\psi + X$

A. J/ψ mass distributions in the $\Upsilon(1S)$ data

Figure 2 shows the invariant mass distribution of J/ψ candidates for (a) $J/\psi \rightarrow \mu^+\mu^-$ and (b) $J/\psi \rightarrow e^+e^-$ in the $\Upsilon(1S)$ on-resonance sample satisfying all selection criteria. The shaded histograms show the corresponding distributions for $\Upsilon(4S)$ continuum data, scaled by a factor of 0.65, which accounts for the differences in luminosities and center-of-mass energies. The mass distributions from the $\Upsilon(1S)$ data set are fit to the sum of a linear background and a Gaussian signal whose means and widths are allowed to float. The fitted peaks have a resolution of 13.4 MeV/c^2 and 14.2 MeV/c^2 for the $J/\psi \rightarrow \mu^+\mu^-$ and $J/\psi \rightarrow e^+e^-$ channels, respectively. The fitted yields are 399 ± 25 $J/\psi \rightarrow \mu^+\mu^-$ and 449 ± 27 $J/\psi \rightarrow e^+e^-$ signals events.

To study the momentum distribution, we divide the data into bins of scaled momentum, x, where $x = p_{J/\psi}/p_{\max}$. Here, $p_{\max} = (1/2\sqrt{s})(s - M^2_{J/\psi})$ is the maximum J/ψ momentum assuming the J/ψ is recoiling against a massless particle, s is the square of the center-of-mass energy, $p_{J/\psi}$ is the momentum of the J/ψ candidate, and $M_{J/\psi}$ is the J/ψ mass [22]. The data are binned in intervals of $\Delta x = 0.2$. This scaled momentum variable removes the beam-energy dependence which is useful in comparing spectra on the $\Upsilon(1S)$ and the $\Upsilon(4S)$. The invariant mass distributions for $J/\psi \rightarrow \mu^+\mu^-$ and $J/\psi \rightarrow e^+e^-$ for $\Upsilon(1S)$ data in bins of x are shown in Figs. 3 and 4, respectively. If the x distribution has a sharp peak near the kinematic end point, there may be smearing into the $x > 1.0$ region. The absence of any signal in the $1.0 \leq x < 1.2$ bin shows that all events are contained within the physically allowed region. A simulation of the J/ψ signal (see Sec. III C) indicates that the widths of the invariant mass distributions are independent of J/ψ momentum, and therefore these distributions are fit using a width fixed to the values obtained from the full sample.

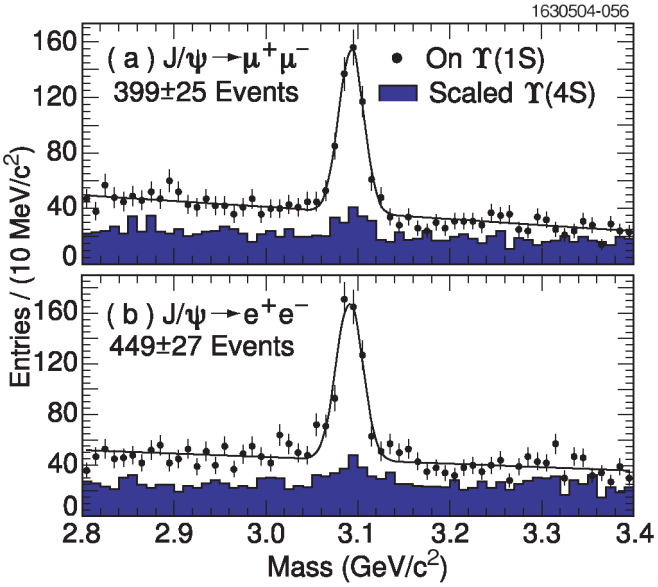

FIG. 2 (color online). Dilepton invariant mass distributions for (a) $J/\psi \rightarrow \mu^+\mu^-$ and (b) $J/\psi \rightarrow e^+e^-$ candidates for data taken on the $\Upsilon(1S)$ resonance (points) and data taken just below the $\Upsilon(4S)$ resonance (shaded). The $\Upsilon(4S)$ distributions are scaled to account for the different integrated luminosities and center-of-mass energies for the two data samples.

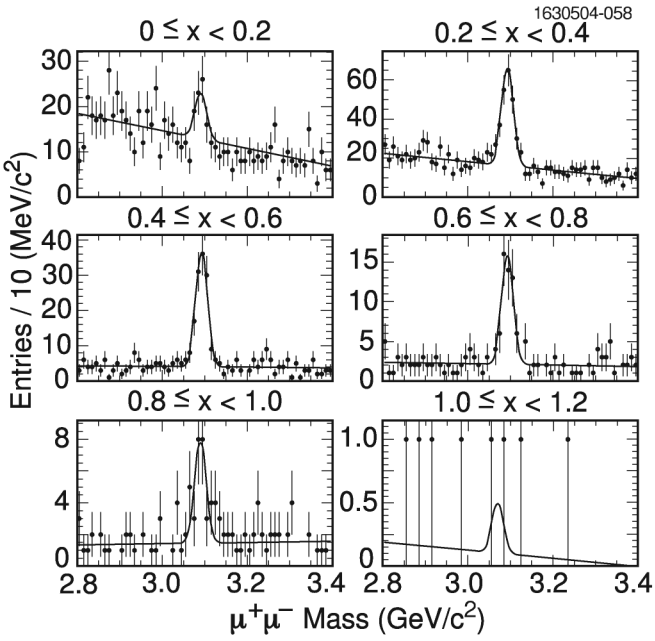

FIG. 3. Invariant mass distributions for $J/\psi \rightarrow \mu^+\mu^-$ candidates in x bins of size 0.2 for data taken on the $\Upsilon(1S)$ resonance.

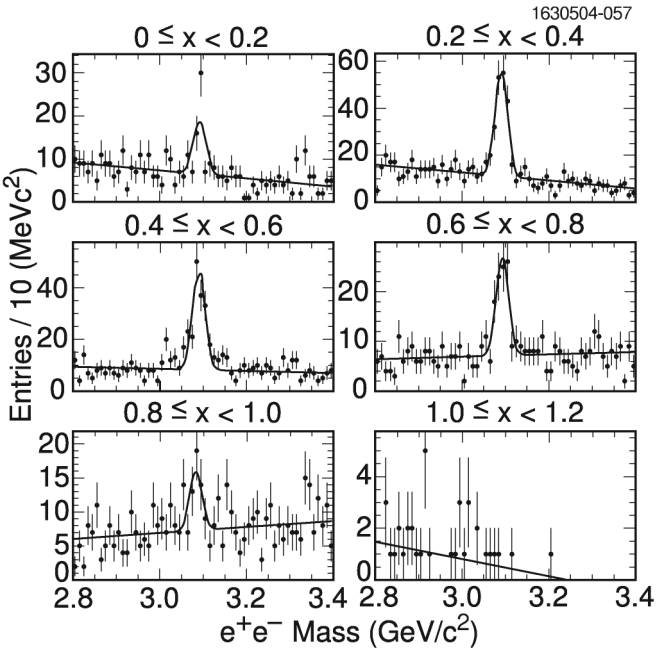

FIG. 4. Invariant mass distributions for $J/\psi \to e^+e^-$ candidates in x bins of size 0.2 for data taken on the $\Upsilon(1S)$ resonance.

B. Candidate J/ψ mass distributions in the $\Upsilon(4S)$ data

The continuum contribution to the $\Upsilon(1S) \to J/\psi + X$ signal is estimated using data taken on and below the $\Upsilon(4S)$. This measurement is interesting in itself in light of the disagreement in the rates for $e^+e^- \to J/\psi + X$ measured by *BABAR* [9] and Belle [10]. We employ the same event selection criteria as for the data taken on the $\Upsilon(1S)$, except that for the on-$\Upsilon(4S)$ data, we require the J/ψ to have momentum larger than 2 GeV/c, which eliminates contributions from B-meson decay.

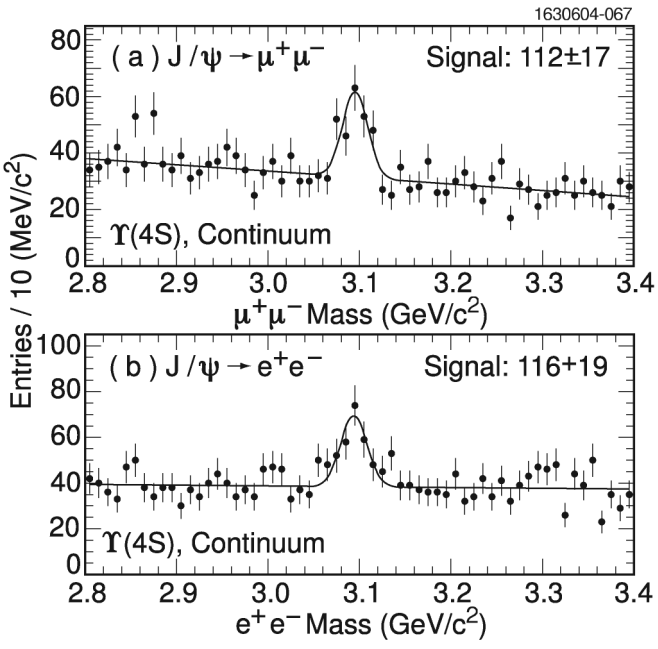

FIG. 5. Invariant mass distribution for (a) $J/\psi \to \mu^+\mu^-$ and (b) $J/\psi \to e^+e^-$ in data taken below the $\Upsilon(4S)$. The data are integrated over all momenta.

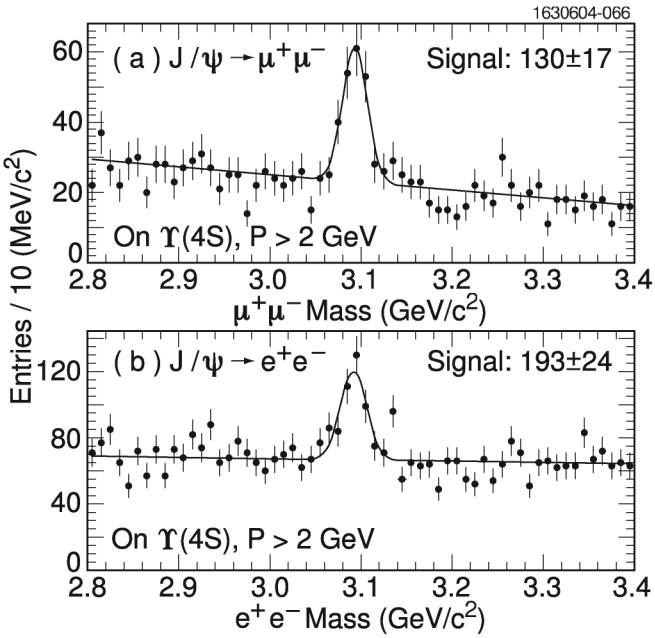

FIG. 6. Invariant mass distributions for (a) $J/\psi \to \mu^+\mu^-$ and (b) $J/\psi \to e^+e^-$ in data taken on the $\Upsilon(4S)$ resonance. To reject J/ψ's from B decay, we require the momentum of the J/ψ to be larger than 2.0 GeV/c.

The measured signal for $e^+e^- \to J/\psi + X$ below the $\Upsilon(4S)$ is shown in Fig. 5 for (a) $J/\psi \to \mu^+\mu^-$ and (b) $J/\psi \to e^+e^-$. The fitted numbers of events are 112 ± 17 ($J/\psi \to \mu^+\mu^-$) and 116 ± 19 ($J/\psi \to e^+e^-$). The corresponding distributions for data taken on the $\Upsilon(4S)$ resonance are shown in Fig. 6. The fitted yields are 130 ± 17 $J/\psi \to \mu^+\mu^-$ and 193 ± 24 $J/\psi \to e^+e^-$ events. The yields per unit luminosity are statistically compatible, after correcting the on-$\Upsilon(4S)$ yield for the 2 GeV/c momentum requirement. The correction is determined from the J/ψ momentum spectrum from the below-$\Upsilon(4S)$ continuum and is estimated to be $(25 \pm 6)\%$.

C. J/ψ reconstruction efficiency

The data are corrected for geometric acceptance and analysis requirements using the PYTHIA Monte Carlo [23] and a GEANT-based detector simulation [24].

The reconstruction efficiency as a function of x and $\cos\theta_{J/\psi}$, where $\theta_{J/\psi}$ is the polar angle of the J/ψ in the lab frame, is shown in Fig. 7. The circular points are for $J/\psi \to \mu^+\mu^-$ and the triangles are for $J/\psi \to e^+e^-$. The efficiencies decrease slightly with increasing momentum and $|\cos\theta_{J/\psi}|$ and have average values of $(40 \pm 2)\%$ for $J/\psi \to \mu^+\mu^-$ and $(50 \pm 2)\%$ for $J/\psi \to e^+e^-$. The small drop in efficiency with momentum is a result of not reconstructing the softer lepton which is emitted

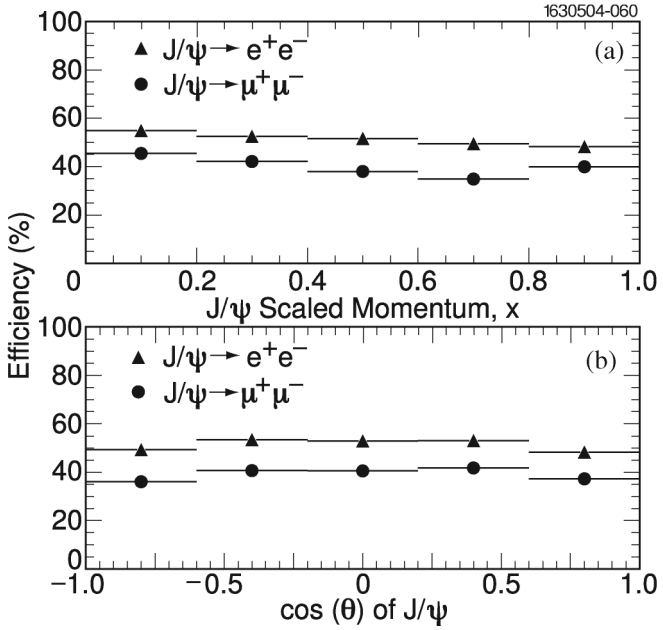

FIG. 7. Efficiency for reconstructing J/ψ's in $\Upsilon(1S)$ decays as a function of (a) scaled J/ψ momentum, and (b) $\cos\theta_{J/\psi}$. The circles are for $J/\psi \to \mu^+\mu^-$ and the triangles are for $J/\psi \to e^+e^-$.

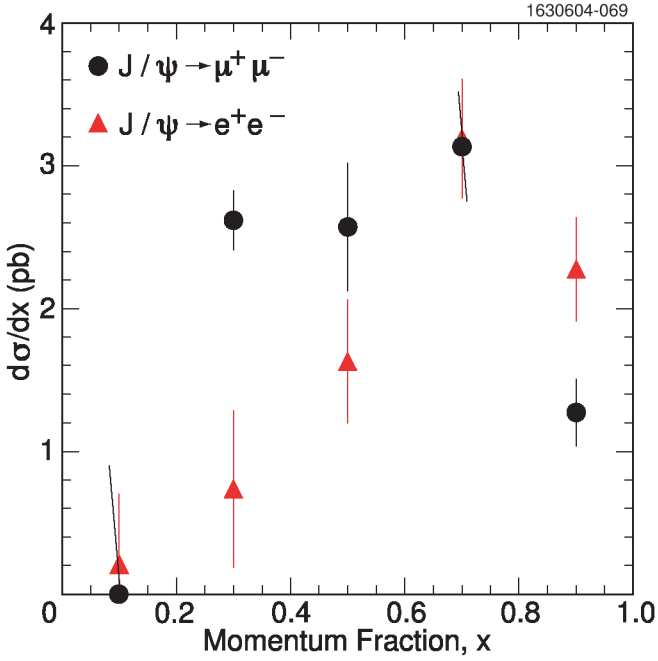

FIG. 8 (color online). Distributions in x for $e^+e^- \to J/\psi + X$ using the combined data taken on and just below the $\Upsilon(4S)$. The circles show the results obtained using $J/\psi \to \mu^+\mu^-$ and the triangles show the corresponding distribution obtained using $J/\psi \to e^+e^-$.

backward in the J/ψ rest frame. The lower $J/\psi \to \mu^+\mu^-$ reconstruction efficiency is due to the requirement that both muons penetrate at least three layers of iron absorber, which limits the muon momentum to be larger than about 1 GeV/c.

The momentum distributions of both the $\Upsilon(1S) \to J/\psi + X$ signal as well as the on-$\Upsilon(4S)$ and below-$\Upsilon(4S)$ yields are corrected using these x-dependent efficiencies. This is justified since the reconstruction efficiency is not sensitive to small differences in the event environment [between $\Upsilon(1S) \to J/\psi + X$ and $e^+e^- \to J/\psi + X$]. Continuum-produced J/ψ's have a similar charged-track multiplicity to $\Upsilon(1S) \to J/\psi + X$ ($\approx$7–8) and the $\Upsilon(1S)$ data peak at low R_2 (see Sec. III H, and figures therein) as do R_2 measurements in the continuum [see Figs. 1(c) and 1(d) in Ref. [9]].

D. Corrected J/ψ momentum distributions on and just below the $\Upsilon(4S)$ resonance

The resulting differential cross sections, $d\sigma/dx$, versus x, are shown in Fig. 8 using the combined on-$\Upsilon(4S)$ and below-$\Upsilon(4S)$ data. The circles represent $J/\psi \to \mu^+\mu^-$ and the triangles are $J/\psi \to e^+e^-$. The distributions clearly peak at large x values with a mean of about 0.7. Integrating these distributions, and using $\mathcal{B}(J/\psi \to l^+l^-) = 5.9\%$ [22], we find $\sigma(e^+e^- \to J/\psi + X) = 2.0 \pm 0.2(\text{stat})$ pb for $J/\psi \to \mu^+\mu^-$ and $\sigma(e^+e^- \to J/\psi + X) = 1.7 \pm 0.2(\text{stat})$ pb for $J/\psi \to e^+e^-$. Combining these results we obtain $\sigma(e^+e^- \to J/\psi + X) = 1.9 \pm 0.2(\text{stat})$ pb. The results using the different lepton species are consistent with one another and lie between the *BABAR* and Belle measurements of $(2.52 \pm 0.21 \pm 0.21)$ pb and $(1.47 \pm 0.10 \pm 0.13)$ pb, respectively. The rates found in the continuum are about a factor of 6–7 lower than on the $\Upsilon(1S)$.

E. Extrapolation of the $\Upsilon(4S)$ results to the $\Upsilon(1S)$

The extrapolation of the differential cross section for $e^+e^- \to J/\psi + X$ on and below the $\Upsilon(4S)$ (see Fig. 8) to the $\Upsilon(1S)$ requires that we take into account the differences between these two samples and includes two factors (other than the luminosity scaling): the ratio of partonic cross sections for $e^+e^- \to J/\psi + X$ and a phase space correction for producing the $J/\psi + X$ final state. For the former, we assume $1/s$ scaling, since the process proceeds through a virtual photon, and therefore the parton-level cross section at 9.46 GeV is 1.25 times larger than at 10.58 GeV. For the phase space extrapolation, we bound this factor at unity by assuming the phase space at 9.46 GeV is equal to that at 10.58 GeV. To obtain a lower bound, we assume that the J/ψ's are always produced in association with a pair of D mesons, which has a significantly reduced phase space at 9.46 GeV as compared to 10.58 GeV. Using PYTHIA, we determine that the probability of producing $J/\psi D\bar{D}$ at 9.46 GeV is 55% of the corresponding value at 10.58 GeV. Using these values as extremes, and assuming that the "true" value has a flat probability of lying somewhere in that interval, we esti-

mate the phase space ratio is 0.78 ± 0.13. Combining the two factors, we determine the continuum extrapolation factor, $f_{\rm cont} = 0.98 \pm 0.16$.

For the J/ψ momentum spectrum in $\Upsilon(1S)$ decays, we are primarily interested in the shape for the gluonic intermediate states. The $q\bar{q}$ intermediate state, which proceeds through the coupling of the $\Upsilon(1S)$ to a virtual photon, is assumed to have the same shape in x as in $e^+e^- \to J/\psi + X$, and therefore is more closely related to the predictions for J/ψ production in the continuum. Therefore for the purposes of the momentum spectrum, we subtract the expected $\Upsilon(1S) \to \gamma^* \to q\bar{q} \to J/\psi + X$ contribution. This contribution is included for the branching fraction measurement. Any potential interference between the continuum and the $\Upsilon(1S) \to \gamma^* \to q\bar{q}$ contributions is neglected. We express the $\Upsilon(1S) \to \gamma^* \to q\bar{q}$ rate relative to the corresponding rate for $e^+e^- \to J/\psi + X$ using

$$\frac{\sigma_{\Upsilon(1S)\to q\bar{q}}}{\sigma_{e^+e^-\to q\bar{q}}} = \frac{R \times \sigma_{\Upsilon(1S)\to\mu^+\mu^-}}{R \times \sigma_{e^+e^-\to\mu^+\mu^-}} = \frac{\sigma_{\Upsilon(1S)\to\mu^+\mu^-}}{\sigma_{e^+e^-\to\mu^+\mu^-}}. \quad (1)$$

Here, $\sigma_{\Upsilon(1S)\to X}$ is shorthand for $\sigma(e^+e^- \to \Upsilon(1S)) \times \mathcal{B}(\Upsilon(1S) \to X)$. The measured value for $\sigma_{\Upsilon(1S)\to\mu^+\mu^-}$ is 0.555 ± 0.022 nb [25]. In that same reference, the theoretical value for $\sigma_{e^+e^-\to\mu^+\mu^-}$ at 9.46 GeV is estimated to be 1.12 nb [25]. A more recent estimate based on the FPAIR MC simulation [26] gives a larger cross section of about 1.38 nb. Taking the average of these two cross sections as our central value and half their difference as the uncertainty, we obtain $\sigma_{e^+e^-\to\mu^+\mu^-} = 1.25 \pm 0.13$ nb. We therefore estimate that the $\Upsilon(1S) \to \gamma^* \to q\bar{q} \to J/\psi + X$ contribution is $(44 \pm 5)\%$ of the $e^+e^- \to J/\psi + X$ at $\sqrt{s} = 9.46$ GeV. Adding this contribution to the continuum extrapolation factor, $f_{\rm cont}$, we obtain an overall extrapolation factor for the x spectrum of $f_x = 1.41 \pm 0.18$.

F. Corrected J/ψ momentum distributions and branching fractions in $\Upsilon(1S)$ data

Figure 9 shows the differential cross sections in x for (a) $J/\psi \to \mu^+\mu^-$ and (b) $J/\psi \to e^+e^-$ using data taken on the $\Upsilon(1S)$ (solid circles) and averaged results from the data taken on and below the $\Upsilon(4S)$ (triangles). The latter have been scaled as discussed above to include both the continuum and $\Upsilon(1S) \to \gamma^* \to q\bar{q}$ contributions. The differential cross section (versus x) for $\Upsilon(1S) \to J/\psi + X$ is given by the difference of these two distributions and reflects only the contributions from gluonic intermediate states. The results are shown in Fig. 10 using $J/\psi \to \mu^+\mu^-$ (circles) and $J/\psi \to e^+e^-$ (triangles). The figure also shows the theoretical predictions of the color-octet [15] (solid line) and the color-singlet $\Upsilon(1S) \to J/\psi + c\bar{c}g$ [13] (dashed line) model.

The branching fraction for $\Upsilon(1S) \to J/\psi + X$ is computed by integrating the differential cross section distribution. We subtract only the expected continuum contribution (we use $f_{\rm cont}$ as our extrapolation factor as opposed to f_x), so that the branching fraction includes the three intermediate hadronic states: ggg, $gg\gamma^{(*)}$, and $q\bar{q}$. The resulting branching fractions for the $J/\psi \to \mu^+\mu^-$ and $J/\psi \to e^+e^-$ final states are

$$\mathcal{B}_{\mu\mu}(\Upsilon(1S) \to J/\psi + X) = (6.9 \pm 0.5(\text{stat})) \times 10^{-4},$$
$$\mathcal{B}_{ee}(\Upsilon(1S) \to J/\psi + X) = (6.1 \pm 0.5(\text{stat})) \times 10^{-4}. \quad (2)$$

Systematic uncertainties are presented in Sec. VI. Using $\Gamma_{\rm tot}(\Upsilon(1S)) = (53.0 \pm 1.5)$ keV [22], our measurement corresponds to partial widths, $\Gamma_{ggg+gg\gamma+q\bar{q}}$ of (36.6 ± 2.8) eV and (32.3 ± 2.8) eV for the $J/\psi \to \mu^+\mu^-$ and $J/\psi \to e^+e^-$ channels, respectively.

Subtracting the expected $\Upsilon(1S) \to \gamma^* \to q\bar{q}$ contribution, we obtain $\Gamma_{ggg+gg\gamma^{(*)}}$ of (33.9 ± 2.8) eV and (30.2 ± 2.3) eV. In other words, about 90% of the J/ψ rate comes from the ggg and $gg\gamma^{(*)}$ intermediate states. The $gg\gamma^{(*)}$ contribution is only expected to be at the level of about 5% [15] of the ggg rate.

Theoretical estimates of this rate based only on color-octet contributions, which neglect the $q\bar{q}$ intermediate state, give a total branching fraction of 6.2×10^{-4} [15,16]. Those predictions are in good agreement with the measurements reported here. On the other hand, our measured momentum spectrum is significantly softer

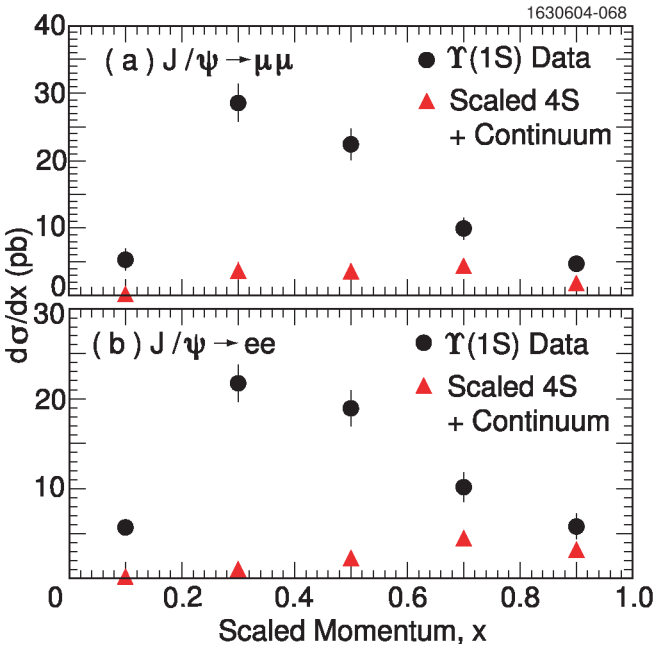

FIG. 9 (color online). Differential cross sections in x for data taken on the $\Upsilon(1S)$ (points) and data taken both on and just below the $\Upsilon(4S)$ (triangles). The latter have been scaled to account for the $\Upsilon(1S) \to \gamma^* \to q\bar{q}$ contribution, as discussed in the text. The upper figure shows the results obtained using $J/\psi \to \mu^+\mu^-$ and the lower figure shows the corresponding distributions obtained using $J/\psi \to e^+e^-$.

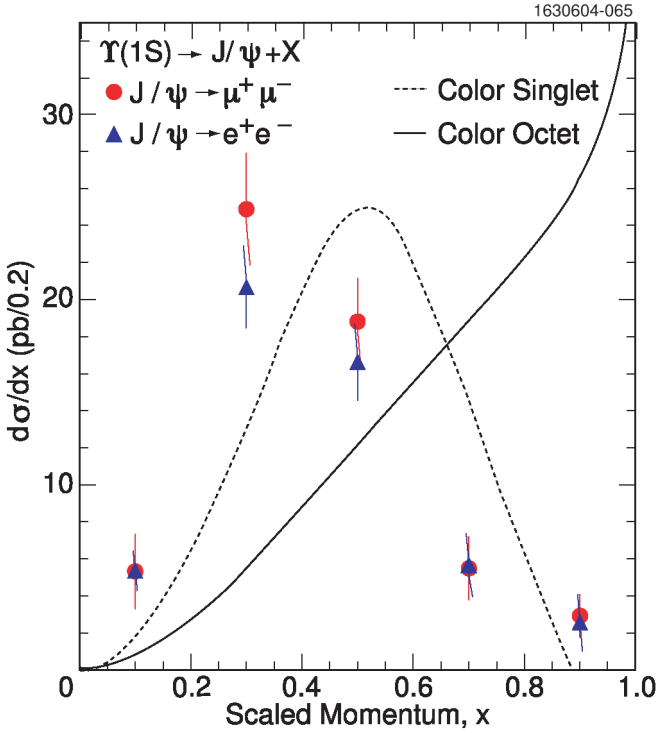

FIG. 10 (color online). Differential cross sections in x for $\Upsilon(1S) \to J/\psi + X$ obtained using $J/\psi \to \mu^+\mu^-$ (circles) and $J/\psi \to e^+e^-$ (triangles). We also show the theoretical expectations based on the color-octet (solid line) [15] and color-singlet (dashed line) [13] models.

than predicted by the color-octet model, which is expected to peak near the kinematic limit (see Fig. 10). However, it has been recently pointed out [11] that in a similar process, $e^+e^- \to J/\psi + X$, the nonrelativistic calculations break down near the kinematic end point where there are large perturbative and nonperturbative corrections. These effects may be systematically treated using the so-called SCET and are expected to soften the J/ψ momentum spectrum. Using SCET, the shape of the measured J/ψ momentum spectrum in $e^+e^- \to J/\psi + X$, which peaks near $x \simeq 0.7$, was shown to be reproducible [11]. It will be interesting to see if these corrections, when applied to $\Upsilon(1S) \to J/\psi + X$, can soften the color-octet predictions sufficiently to bring them into agreement with our data.

Our measured rate is also consistent with the predictions of the color-singlet process $\Upsilon(1S) \to J/\psi c\bar{c}g + X$, which predicts a branching fraction of 5.9×10^{-4} and a soft momentum spectrum which peaks at $x \approx 0.5$ and has a kinematic limit of $x < 0.9$. While the data are somewhat softer than the color-singlet predictions, it should be noted that this is a parton-level calculation and neglects the hadronization process. Inclusion of the hadronization of the charm quarks to charm hadrons softens the J/ψ momentum spectrum, with more softening occurring as the mass of the recoiling system increases. Further softening of the J/ψ momentum spectrum occurs when including the feed-down of $\psi(2S)$ and χ_{cJ} to J/ψ. Using a PYTHIA simulation of the color-singlet process, we are able to obtain reasonably good agreement in the $x < 0.6$ region using our measured values for the feed-down from $\psi(2S)$, χ_{cJ} to J/ψ along with a reasonable, but arbitrary admixture of recoiling D, D^*, and D^{**} states. This is not necessarily evidence for color-singlet production, but it is suggestive.

G. J/ψ angular distributions in $\Upsilon(1S)$ data

Angular distributions have the potential to differentiate the mechanisms for J/ψ production in e^+e^- collisions. Theoretical predictions for the production and helicity angle distributions for continuum production are available [8,27,28], but the calculations are yet to be done for $\Upsilon(1S)$ decay.

In the same spirit, we present distributions of the (polar) production angle, $\cos\theta_{J/\psi}$, of the J/ψ and the helicity angle, $\cos\theta_{\rm hel}$, where $\theta_{\rm hel}$ is the angle between the positive lepton momentum in the J/ψ rest frame and the J/ψ momentum in the lab frame. The efficiency-corrected $J/\psi \to \mu^+\mu^-$ and $J/\psi \to e^+e^-$ channels are combined and shown in Fig. 11. Here, we subtract the expected $\Upsilon(1S) \to \gamma^* \to q\bar{q}$ and continuum contributions to extract the ggg and $gg\gamma^{(*)}$ shapes. The normalizations are arbitrary. The top figure shows the distribution of

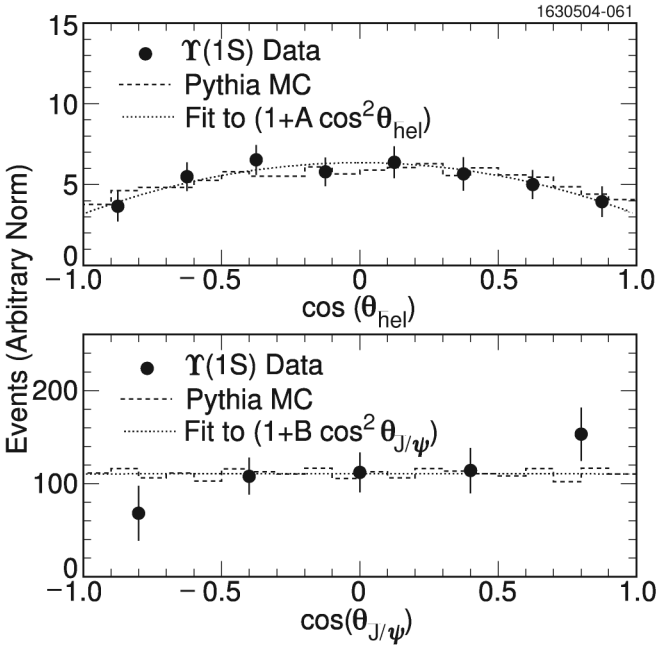

FIG. 11. The helicity angular distributions, $\cos\theta_{\rm hel}$ (top panel) and production angle, $\cos\theta_{J/\psi}$ (bottom panel) of the J/ψ in $\Upsilon(1S) \to J/\psi + X$. In each case, the points are the $\Upsilon(1S)$ data, the dashed histogram is a PYTHIA simulation of $\Upsilon(1S) \to J/\psi + X$, and the dotted line is a fit to the $\Upsilon(1S)$ data as described in the text.

$\cos\theta_{\rm hel}$ for $\Upsilon(1S)$ data (points), PYTHIA simulation (dashed line), and a fit (dotted line) to the form $(1 + A\cos^2\theta_{\rm hel})$, from which we find $A = -0.48 \pm 0.16$ (χ^2/d.o.f. = 0.50). The bottom figure shows the distribution in $\cos\theta_{J/\psi}$ for $\Upsilon(1S)$ data (points), PYTHIA simulation (dashed line) and a fit (dotted line) to the form $(1 + B\cos^2\theta_{J/\psi})$, from which we find $B = 0.01 \pm 0.16$ (χ^2/d.o.f. = 1.44). The functional forms are the same as those used to describe the angular distributions for continuum production of J/ψ mesons [8,28]. The negative value of A indicates that the J/ψ has a significant longitudinal polarization component (a positive value would indicate transverse polarization). For continuum production of J/ψ, the color-octet and color-singlet models differ greatly on their expectations for B at large values of scaled momentum, with $B \simeq -0.85$ for the color-singlet model [28] and $B \approx +1$ for the color-octet model [8]. If a large difference persists for $\Upsilon(1S)$ decay, the production angle distribution could be useful in differentiating these two mechanisms. We note that the PYTHIA simulation (using default parameters), which produces J/ψ via $\Upsilon(1S) \to J/\psi + D\bar{D}$, appears to be in reasonable agreement with data.

H. Event-level distributions

Additional information on the $\Upsilon(1S) \to J/\psi + X$ process can be obtained by studying various event-level distributions. We present distributions of

- The number of reconstructed charged tracks, $N_{\rm trk}$ [Fig. 12(a)]
- Reconstructed neutral energy in the crystal calorimeter, $E_{\rm NEU}$ [Fig. 12(b)]
- The second Fox-Wolfram moment, R_2 [Fig. 12(c)]
- Invariant mass recoiling against the J/ψ, $M_{\rm RECOIL}$ [Fig. 12(d)]

In each case, we have performed a sideband subtraction, where the signal region is defined to be from $3.04 < M_{l^+l^-} < 3.14$ GeV/c^2 and the sideband region includes the $M_{l^+l^-}$ regions from 2.90–2.95 and 3.20–3.25 GeV/c^2. The relatively small continuum contribution has not been subtracted. For each distribution, we also show the corresponding distribution from the PYTHIA MC simulation, which primarily produces a final state which consists of $J/\psi D\bar{D}$. The data are shown as points ($J/\psi \to \mu^+\mu^-$ are circles and $J/\psi \to e^+e^-$ are triangles) and the simulation is the histogram. We find that the charged particle multiplicity, which includes all charged particles, has a mean of about 9. The neutral energy, which comprises all energy in the calorimeter which is not associated with charged tracks, has an average of about (1.5–2.0) GeV, with most of the events having less than about 3.5 GeV. The Fox-Wolfram moment, R_2, peaks at low R_2 in $\Upsilon(1S) \to J/\psi + X$ data which indicates that these events tend to be more spherical than collimated (jetlike). The recoil mass can be used to discern whether there is another

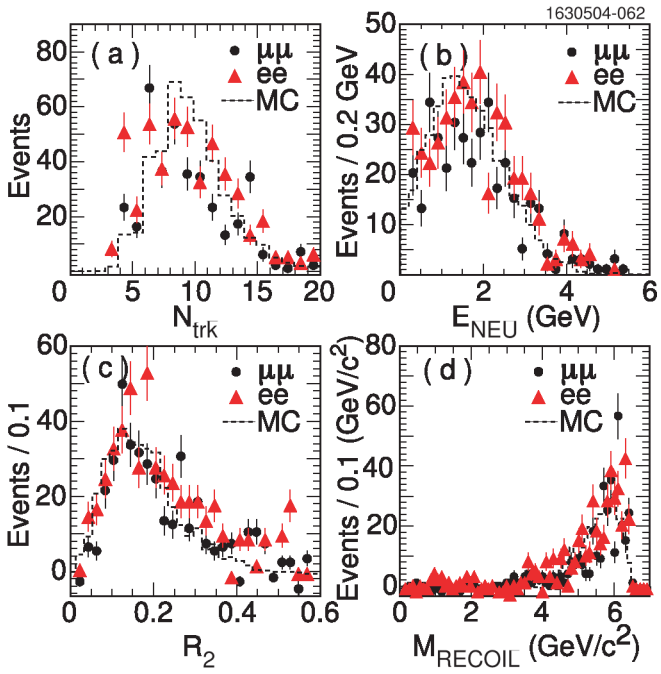

FIG. 12 (color online). Sideband-subtracted distributions of (a) number of charged tracks, $N_{\rm trk}$, (b) neutral energy, $E_{\rm NEU}$, (c) the second Fox-Wolfram moment, R_2, and (d) the recoil mass, $M_{\rm RECOIL}$, for $\Upsilon(1S)$ data and PYTHIA simulation. The points (triangles) correspond to $J/\psi \to \mu^+\mu^-$ ($J/\psi \to e^+e^-$), and the histograms are the corresponding distributions from the simulation.

particle recoiling against the J/ψ. It is defined by

$$M_{\rm RECOIL} = \sqrt{(\sqrt{s} - E_{J/\psi})^2 - p^2_{J/\psi}}, \qquad (3)$$

where s is the square of the center-of-mass energy, and $p_{J/\psi}$ and $E_{J/\psi}$ are the momentum and energy of the J/ψ candidate. We do not observe any significant peaks in the recoil mass spectrum, indicating that the J/ψ is usually not accompanied only by a second (bound) $c\bar{c}$ meson. The color-octet model predicts ~1% contribution to the inclusive rate whereas the color-singlet model does not predict the fraction of recoiling charm which is in the form of charmonium.

I. Cross-check using $B \to J/\psi + X$

As a cross-check of our detector simulation and analysis procedure, we use the same tools to measure $\mathcal{B}(B \to J/\psi + X)$ in $\Upsilon(4S)$ data. The efficiencies for reconstructing J/ψ in $B \to J/\psi + X$ events are about 5% lower than in $\Upsilon(1S) \to J/\psi + X$. In addition to the selection requirements described in Sec. II, we require the J/ψ momentum to be less than 2.0 GeV/c. The yields are corrected for the expected continuum contribution, which is typically at the level of 1%–2% of the $B \to J/\psi + X$ yield. The resulting branching fractions are found to be $[1.17 \pm 0.03(\text{stat})]\%$ and $[1.14 \pm 0.02(\text{stat})]\%$ for $J/\psi \to \mu^+\mu^-$

and $J/\psi \to e^+e^-$, respectively. These results are slightly higher than the world average value of $(1.090 \pm 0.035)\%$ [22]. This difference is included as a systematic uncertainty in the J/ψ reconstruction efficiency.

IV. MEASUREMENTS OF $\Upsilon(1S) \to \psi(2S) + X$

A. Measurements in $\Upsilon(1S)$ data

We search for $\Upsilon(1S) \to \psi(2S) + X$ using the decay mode $\psi(2S) \to J/\psi\pi^+\pi^-$. Pion candidates must pass the previously mentioned track selection criteria and must have a measured energy loss in the tracking chambers within 4 standard deviations of the expected value. Using all pairs of oppositely charged pion candidates, we compute the invariant mass difference, $M(l^+l^-\pi^+\pi^-) - M(l^+l^-)$, a quantity which has better resolution than $M(J/\psi\pi^+\pi^-)$. We also require $M(l^+l^-)$ to be in the range from 3.00–3.14 GeV/c^2. The resulting distribution for $M(l^+l^-\pi^+\pi^-) - M(l^+l^-)$ is shown in Fig. 13, where we have summed over both lepton species. The distribution is fit to the sum of a Gaussian signal shape and a second-order polynomial background. The width of the Gaussian is fixed to 2.5 MeV/c^2, the value determined from $B \to \psi(2S) + X$ data. The 0.3 MeV intrinsic width [22] of the $\psi(2S)$ is negligible compared to the detector resolution and is therefore ignored. The fitted yield is 56 ± 11 events. The significance of the signal, $S/\sqrt{S+B}$, where S is the fitted signal and B is the estimated background, varies from 6–7, depending on whether B is estimated from the sidebands or the background function.

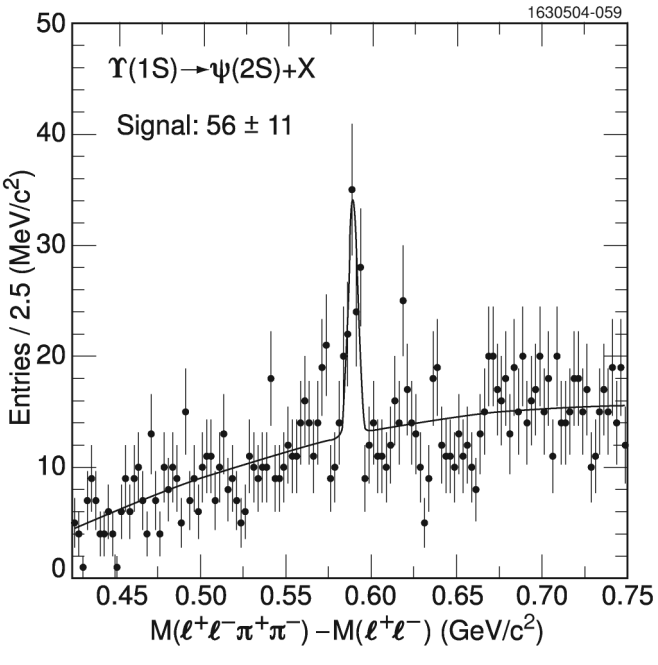

FIG. 13. Invariant mass difference $M(l^+l^-\pi^+\pi^-) - M(l^+l^-)$ for both $J/\psi \to \mu^+\mu^-$ and $J/\psi \to e^+e^-$ candidates with invariant mass in the range from 3.00–3.14 GeV/c^2.

The radiative return background, $e^+e^- \to \psi(2S)\gamma$, is estimated using the EVTGEN [29] simulation package and published cross sections in Ref. [30]. The events are processed using GEANT and analyzed using the same analysis tools as the $\Upsilon(1S)$ data. The efficiency for these events to pass a loose hadronic event selection is $(1.4 \pm 0.1)\%$ for $J/\psi \to \mu^+\mu^-$ decays and $(8.4 \pm 0.6)\%$ for $J/\psi \to e^+e^-$ decays. For these subsamples, a fraction, $f_{\mu\mu}^{\text{radret,pass}} = 0.40 \pm 0.09$ of $J/\psi \to \mu^+\mu^-$ decays also passes the analysis-specific selection criteria discussed in Sec. II. The corresponding fraction for $J/\psi \to e^+e^-$ decays is $f_{ee}^{\text{radret,pass}} = 0.15 \pm 0.02$. The larger efficiency for the electron channel to pass the loose hadronic event selection results from the use of the calorimeter in defining this subsample of events. With the assumption that all data events which fail the analysis requirements are radiative return (discussed below), the expected background contribution in data from radiative return is computed using

$$N_{ll}^{\text{radret}} = \left(\frac{f_{ll}^{\text{radret,pass}}}{f_{ll}^{\text{radret,rej}}}\right)_{\text{MC}} N_{ll}^{\text{data,rej}}, \tag{4}$$

where the quantity in parentheses is the ratio of simulated radiative return events which pass the analysis-specific selection to those that are rejected. The quantity $N_{ll}^{\text{data,rej}}$ is the number of rejected events in $\Upsilon(1S)$ data for each lepton species. We find $N_{\mu\mu}^{\text{data,rej}} = 5$ and $N_{ee}^{\text{data,rej}} = 39$ in the $\psi(2S)$ signal region, obtained through sideband subtraction. We therefore estimate radiative return contributions of 2.0 ± 1.0 events and 5.9 ± 1.0 events in the $J/\psi \to \mu^+\mu^-$ and $J/\psi \to e^+e^-$ channels, respectively, and therefore a total of 7.9 ± 1.4 background events from this source.

The assumption that the rejected events in data are from radiative return is supported by comparing event-level distributions of these rejected events between data and simulated $e^+e^- \to \psi(2S)\gamma$ radiative return events. Figure 14 shows comparisons of (a) the number of reconstructed charged tracks, N_{trk}, (b) neutral energy in the calorimeter, E_{NEU}, (c) missing event momentum, P_{event}, and (d) the cosine of the angle between the $\psi(2S)$ direction and the beam axis, $\cos\theta_{\psi(2S)}$. In all cases, the radiative return simulation reproduces the rejected events in $\Upsilon(1S)$ data, indicating that the rejected data events are mostly from radiative return.

In Fig. 15 we show the analogous distributions for $\Upsilon(1S)$ data (points) passing all analysis selection requirements. The corresponding distributions from a MC simulation of $\psi(2S)D\bar{D}$ are overlaid (histogram). These distributions are clearly quite different than the distributions for rejected events (see Fig. 14).

The continuum background contribution is estimated using the measured cross section, $\sigma(e^+e^- \to \psi(2S) + X) = 0.67 \pm 0.09^{+0.09}_{-0.11}$, by Belle [10]. The expected num-

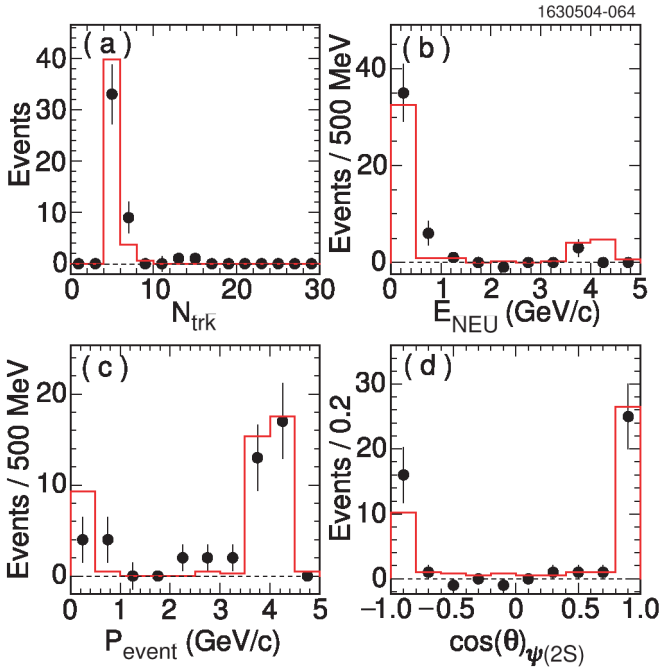

FIG. 14 (color online). Event-level distributions for events rejected in the $\psi(2S)$ analysis. Distributions shown are (a) number of charged tracks, (b) neutral energy, (c) missing event momentum, and (d) cosine of the $\psi(2S)$ production angle. Solid points are rejected $\Upsilon(1S) \to \psi(2S) + X$ candidate events and the histogram is the $e^+e^- \to \psi(2S) + X$ radiative return simulation.

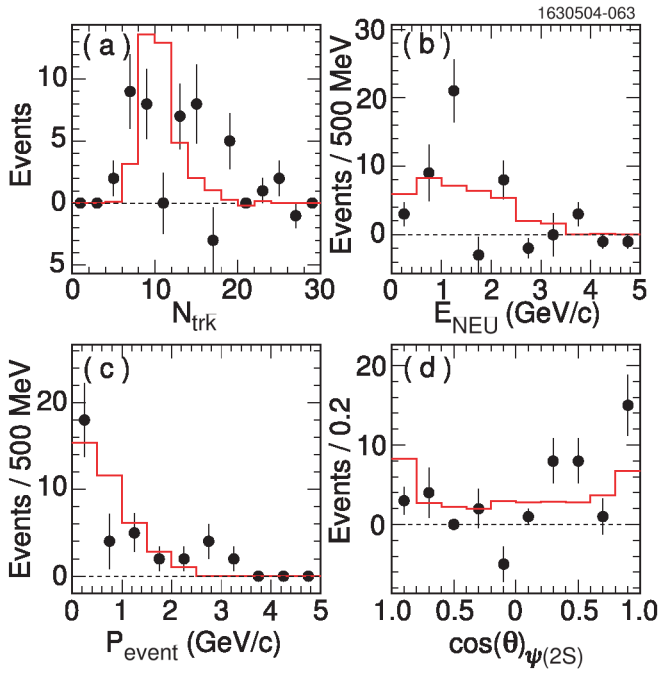

FIG. 15 (color online). Event-level distributions for events accepted in the $\psi(2S)$ analysis. Distributions shown are (a) number of charged tracks, (b) neutral energy, (c) missing event momentum, and (d) cosine of the $\psi(2S)$ production angle. Solid points are accepted $\Upsilon(1S) \to \psi(2S) + X$ candidate events and the histogram is a $\Upsilon(1S) \to \psi(2S) D\bar{D}$ MC simulation.

ber of $\psi(2S)$ continuum background events is then given by

$$N^{\psi(2S)}_{\text{back,exp}} = \sigma(e^+e^- \to \psi(2S) + X) \times \mathcal{L} \times \mathcal{B}(\psi(2S) \times J/\psi\pi^+\pi^-) \times \mathcal{B}(J/\psi \times l^+l^-) \times \epsilon^{\psi(2S)}_{ll} \times f_{\text{cont}}. \quad (5)$$

We use the integrated luminosity $\mathcal{L} = 1.2\ \text{fb}^{-1}$ and branching ratios of $\mathcal{B}(\psi(2S) \to J/\psi\pi^+\pi^-) = 0.318 \pm 0.010$ [22] and $\mathcal{B}(J/\psi \to l^+l^-) = 0.059 \pm 0.001$. The reconstruction efficiencies are determined using a PYTHIA simulation of $\Upsilon(1S) \to \psi(2S) + X$ which is used to model the continuum as well as the signal, for the same reasons as mentioned previously. The efficiencies for both $J/\psi \to \mu^+\mu^-$ and $J/\psi \to e^+e^-$ final states are nearly independent of momentum with average values, $\epsilon^{\psi(2S)}_{ll} = (17 \pm 1)\%$ for $l = \mu$ and $(23 \pm 1)\%$ for $l = e$. For the background extrapolation, we have assumed the same phase space suppression for $\psi(2S)$ as J/ψ and assign a 50% uncertainty to its value. We therefore expect a continuum background contribution of 2.5 ± 1.3 $J/\psi \to \mu^+\mu^-$ and 3.4 ± 1.8 $J/\psi \to e^+e^-$ events, which sum to 5.9 ± 2.2 events. The error is dominated by the uncertainties in $\sigma(e^+e^- \to \psi(2S) + X)$ and f_{cont}. As a consistency check, we have searched our $2.3\ \text{fb}^{-1}$ continuum data sample for $\psi(2S)$, and we find $2.6^{+4.0}_{-2.6}$ and 12 ± 4 events in the $\mu\mu$ and ee channels, respectively. Using the Belle cross section measurement, we would have expected 4.8 ± 0.7 $\mu\mu$ and 6.5 ± 1.0 ee events, which is consistent with our observations.

Combining the radiative return and continuum backgrounds, we estimate a total background of 13.8 ± 2.6 events. The uncertainty in the central value is included as a systematic uncertainty (see Sec. VI).

We now compute $\mathcal{B}(\Upsilon(1S) \to \psi(2S) + X)$. To reduce systematic uncertainty, the $\psi(2S)$ branching fraction is computed relative to $\mathcal{B}(\Upsilon(1S) \to J/\psi + X)$ and is given by

$$\frac{\mathcal{B}(\Upsilon(1S) \to \psi(2S) + X)}{\mathcal{B}(\Upsilon(1S) \to J/\psi + X)} = \frac{1}{\mathcal{B}(\psi(2S) \to J/\psi\pi^+\pi^-)} \times \left(\frac{N^{\psi(2S)}_{ll,\text{rec}} - N^{\psi(2S)}_{ll,\text{back}}}{N^{J/\psi}_{ll,\text{rec}} - N^{J/\psi}_{ll,\text{back}}}\right)\left(\frac{\epsilon^{J/\psi}_{ll}}{\epsilon^{\psi(2S)}_{ll}}\right), \quad (6)$$

where $N^{\psi(2S)}_{ll,\text{rec}}$ ($N^{J/\psi}_{ll,\text{rec}}$) is the total number of $\psi(2S)$ (J/ψ) signal candidates for lepton species $l = e$ and $l = \mu$, $N^{\psi(2S)}_{ll,\text{back}}$ ($N^{J/\psi}_{ll,\text{back}}$) is the expected $\psi(2S)$ (J/ψ) background, and $\epsilon^{\psi(2S)}_{ll}$ ($\epsilon^{J/\psi}_{ll}$) is the average reconstruction efficiency for $\psi(2S)$ (J/ψ). A summary of the inputs used for the $\Upsilon(1S) \to \psi(2S) + X$ branching fraction computation is presented in column four of Table I. The table also shows

TABLE I. Various quantities relevant to the $\psi(2S)$ analysis as discussed in the text. Quantities included are the number of reconstructed candidates J/ψ and $\psi(2S)$ candidates, their expected backgrounds, and efficiencies. The bottom two lines give the computed ratio of branching fractions, as discussed in the text.

Quantity	$\mu\mu$	ee	Combined ($ee + \mu\mu$)
$N^{J/\psi}_{ll\text{rec}}$	399 ± 25	449 ± 27	848 ± 37
$N^{J/\psi}_{ll\text{back}}$	53 ± 11	66 ± 13	119 ± 17
$\epsilon^{J/\psi}_{ll}$	$(40 \pm 2)\%$	$(50 \pm 2)\%$	$(45 \pm 2)\%$
$N^{\psi(2S)}_{ll\text{rec}}$	21 ± 7	35 ± 8	56 ± 11
$N^{\psi(2S)}_{ll\text{back}}$	4.5 ± 1.6	9.3 ± 2.0	13.8 ± 2.6
$\epsilon^{\psi(2S)}_{ll}$	$(17 \pm 1)\%$	$(23 \pm 1)\%$	$(20 \pm 1)\%$
$\frac{\mathcal{B}(\Upsilon(1S)\to\psi(2S)+X)}{\mathcal{B}(\Upsilon(1S)\to J/\psi+X)}$	0.35 ± 0.15	0.46 ± 0.15	0.41 ± 0.11
$\frac{\mathcal{B}(\Upsilon(1S)\to\psi(2S)+X)\mathcal{B}(\psi(2S)\to J/\psi+X)}{\mathcal{B}(\Upsilon(1S)\to J/\psi+X)}$	0.20 ± 0.09	0.27 ± 0.09	0.24 ± 0.06

in columns two and three the values for the $J/\psi \to \mu^+\mu^-$ and $J/\psi \to e^+e^-$ channels separately. The event yields are consistent with one another.

In Table I, the number of J/ψ background events in the $\Upsilon(1S)$ data is computed using the average measured cross section for $e^+e^- \to J/\psi + X$ of (1.9 ± 0.2) pb, the average efficiencies (also shown in Table I), and the continuum extrapolation factor f_{cont} discussed in Sec. III E. The ratio of branching fractions is computed to be

$$\frac{\mathcal{B}(\Upsilon(1S) \to \psi(2S) + X)}{\mathcal{B}(\Upsilon(1S) \to J/\psi + X)} = 0.41 \pm 0.11(\text{stat}). \quad (7)$$

That is, we find that the rate for $\Upsilon(1S) \to \psi(2S) + X$ is $(41 \pm 11)\%$ of the rate for $\Upsilon(1S) \to J/\psi + X$ (systematic uncertainties are discussed in Sec. VI). It is interesting to note that in the $\Upsilon(4S)$ continuum, Belle finds this ratio to be about 0.45 [10] with about a 20% relative uncertainty. Using $\mathcal{B}(\psi(2S) \to J/\psi + X) = (57.9 \pm 1.9)\%$ [22], we find the feed-down contribution of $\psi(2S)$ to $\Upsilon(1S) \to J/\psi + X$ to be

$$\frac{\mathcal{B}(\Upsilon(1S) \to \psi(2S) + X)\mathcal{B}(\psi(2S) \to J/\psi + X)}{\mathcal{B}(\Upsilon(1S) \to J/\psi + X)} = 0.24 \pm 0.06(\text{stat}). \quad (8)$$

This ratio is significantly higher than the expectations of either the color-octet model [15] or the color-singlet model in Ref. [13], each which predict a feed-down rate to be about 10%.

B. Cross-check by measuring $B \to \psi(2S) + X$ in $\Upsilon(4S)$ data

As a cross-check on our analysis, we measure the yield for $B \to \psi(2S) + X$ using 10.4×10^6 B-meson decays from the $\Upsilon(4S)$ data sample and use the same simulation tools to translate this into a branching fraction. The analysis techniques are also identical, except that we additionally require the momentum of the $\psi(2S)$ to be less than 1.5 GeV/c, which is the kinematic limit for its production in B-meson decay. We find 129 ± 16 and 144 ± 18 signal events in the $J/\psi \to \mu^+\mu^-$ and $J/\psi \to e^+e^-$ channels, respectively, of which 3 ± 1 and 4 ± 1 events are expected from continuum background. The efficiencies are determined using generated PYTHIA $b\bar{b}$ events followed by a full detector simulation, and they are found to be $(18 \pm 2)\%$ for the $J/\psi \to \mu^+\mu^-$ channel and $(24 \pm 2)\%$ for the $J/\psi \to e^+e^-$ channel. The branching fractions are measured to be $[3.6 \pm 0.4(\text{stat})] \times 10^{-3}$ for the $J/\psi \to \mu^+\mu^-$ channel and $[3.0 \pm 0.4(\text{stat})] \times 10^{-3}$ for the $J/\psi \to e^+e^-$ channel. Thus we obtain good agreement with the world average value of $(3.10 \pm 0.24) \times 10^{-3}$ [22].

V. MEASUREMENTS OF χ_{cJ} IN $\Upsilon(1S)$ AND $\Upsilon(4S)$ DATA

A. Measurement of $\mathcal{B}(\Upsilon(1S) \to \chi_{cJ} + X)$

We search for $\Upsilon(1S) \to \chi_{cJ} + X$ by reconstructing the $\chi_{cJ} \to J/\psi\gamma$ decay. Photon candidates are required to have energy $E_\gamma > 100$ MeV, not be matched to a charged track and have a shower shape consistent with that of a photon. We also require that the invariant mass of this photon with any other photon in the event is greater than 2.5 standard deviations away from the π^0 mass of 135 MeV/c^2 [22]. Photon candidates passing these selection criteria are combined with J/ψ candidates to form a χ_c candidate. As done previously, we compute mass differences, $M(l^+l^-\gamma) - M(l^+l^-)$, for J/ψ candidates which have a mass in the range $3.00 < M(l^+l^-) < 3.14$ GeV/c^2. From this distribution, we subtract the analogous distribution obtained from the J/ψ sidebands, here defined as candidates with $2.88 < M(l^+l^-) < 2.95$ GeV/c^2 or $3.20 < M(l^+l^-) < 3.27$ GeV/c^2. As was done for the $\psi(2S)$, we combine and average the $J/\psi \to \mu^+\mu^-$ and $J/\psi \to e^+e^-$ channels. The invariant mass difference distribution, $M_{l^+l^-\gamma} - M_{l^+l^-}$, is shown in Fig. 16. The

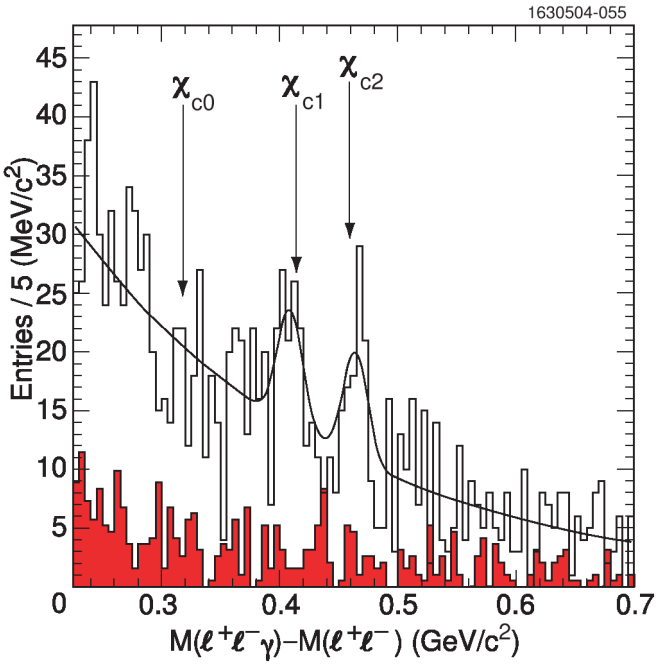

FIG. 16 (color online). Difference of invariant masses, $M(l^+l^-\gamma) - M(l^+l^-)$, for $M(l^+l^-)$ in the range from 3.00 to 3.14 GeV/c^2 for $l = \mu, e$ combined. The solid histogram represents the $\Upsilon(1S)$ data and the shaded histogram is the below-$\Upsilon(4S)$ data scaled by the ratio of luminosities. The arrows indicate the mass differences corresponding to the three χ_c states.

solid histogram is the $\Upsilon(1S)$ data and the shaded histogram is the $\Upsilon(4S)$ continuum, scaled by the ratio of luminosities. The $\Upsilon(1S)$ data is fit using three Gaussians on top of an exponential background. The Gaussian means are restricted to lie within 5 MeV/c^2 of the world average values of the differences between the χ_{cJ} and J/ψ masses (see Table II) [22] and the widths are constrained to the values found from simulation: 12.5, 10.5, and 10.3 MeV/c^2 for $J = 0$, 1, and 2. The larger width for $J = 0$ is a result of the 16.2 MeV intrinsic width which is included in the simulation. The fitted yields are 0 ± 13, 52 ± 12, and 47 ± 11 events for $J = 0$, 1, and 2, respectively. The significance of each signal is given by $S/\sqrt{B}$, where S is the signal yield, and B is the estimated background within ± 3 standard deviations of the fitted mean using the exponential background function. The significances are found to be 3.9 and 4.1 for the $J = 1$ and $J = 2$ states, respectively. The averaged efficiencies for the $J/\psi \to \mu^+\mu^-$ and $J/\psi \to e^+e^-$ channels are $(27 \pm 1)\%$, $(30 \pm 1)\%$, and $(28 \pm 1)\%$ for $J = 0$, 1, and 2 states, respectively. The efficiency for reconstructing the $J = 0$ state includes a $\sim 2\%$ loss of signal events due to events in the tails of the Breit-Wigner. Branching fractions for $\Upsilon(1S) \to \chi_{cJ} + X$ are computed relative to $\Upsilon(1S) \to J/\psi + X$ and are tabulated in Table II. The last column shows the measured fraction of J/ψ's which come from χ_{cJ} feed-down, which is $(11 \pm 3)\%$ for the $J = 1$ state and $(10 \pm 2)\%$ for the $J = 2$ state. We only obtain upper limits on the $J = 0$ state. Theoretical estimates of this ratio are at the level of 10% for the sum of all three χ_{cJ} states [15,17]. The rates we report here are higher than those expectations.

B. Cross-check using $B \to \chi_{cJ} + X$ in $\Upsilon(4S)$ data

As a consistency check, we measure the branching fraction for $\mathcal{B}(B \to \chi_{cJ} + X)$ using 10.4×10^6 B decays from the $\Upsilon(4S)$ data sample. We restrict the χ_{cJ} to have momentum less than 1.6 GeV/c, which is the kinematic limit from B-meson decay. A clear signal is found only for the $J = 1$ state, for which the fitted yield is 347 ± 35 events. The continuum background is negligible and is therefore neglected. The reconstruction efficiency is determined using a $B \to \chi_{cJ} + X$ MC simulation and is found to be $(28 \pm 1)\%$. The branching fraction for $\mathcal{B}(B \to \chi_{c1} + X)$ is thus found to be $[3.3 \pm 0.3(\text{stat})] \times 10^{-3}$, which is consistent with the Particle Data Group (PDG) value of $(3.6 \pm 0.3) \times 10^{-3}$ [22]. The 90% confidence level upper limit on $\mathcal{B}(B \to \chi_{c2} + X)$ is 1.5×10^{-3}, which does not conflict with the measured branching fraction of $(1.3 \pm 0.4) \times 10^{-3}$ [22,31].

VI. ESTIMATES OF SYSTEMATIC UNCERTAINTY

A. Uncertainties in $\Upsilon(1S) \to J/\psi + X$

The branching fractions for $B \to J/\psi + X$ using $J/\psi \to \mu^+\mu^-$ and $J/\psi \to e^+e^-$ were shown in

TABLE II. Measurements of the branching fractions for $\Upsilon(1S) \to \chi_{cJ} + X$ with the relevant inputs. The table includes, from left to right, the χ_{cJ} states, the world average mass difference $M_{\chi_{cJ}} - M_{J/\psi}$, the branching fractions $\mathcal{B}(\chi_{cJ} \to J/\psi\gamma)$, the observed yields, the reconstruction efficiencies, the computed branching fractions relative to $\Upsilon(1S) \to J/\psi + X$, and the computed feed-down to J/ψ. For the χ_{c0} we show 90% confidence level upper limits.

Mode	$M_{\chi_{cJ}} - M_{J/\psi}$ (MeV/c^2)	$\mathcal{B}(\chi_{cJ} \to J/\psi\gamma)$ (%)	N_{events} $(\mu\mu + ee)$	Eff.(%) $(\mu\mu + ee)$	$\frac{\mathcal{B}(\Upsilon(1S)\to\chi_{cJ}+X)}{\mathcal{B}(\Upsilon(1S)\to J/\psi+X)}$ $(\mu\mu + ee)$	Feed-down to J/ψ
χ_{c0}	318	1.11 ± 0.15	0 ± 13	$(27 \pm 1)\%$	<5.9	<0.065
χ_{c1}	414	31.6 ± 2.7	52 ± 12	$(30 \pm 1)\%$	0.35 ± 0.08	0.11 ± 0.03
χ_{c2}	459	20.2 ± 2.0	47 ± 11	$(28 \pm 1)\%$	0.52 ± 0.12	0.10 ± 0.02

Sec. III A to be higher than the world average values by 7% for $J/\psi \to \mu^+\mu^-$ and 5% for $J/\psi \to e^+e^-$, which is taken as the systematic uncertainty in reconstructing these decays. We ascribe an additional uncertainty due to our limited knowledge of the final state in $\Upsilon(1S) \to J/\psi + X$ and its modeling. This additional uncertainty is taken to be half the difference in the reconstruction efficiency obtained from our $\Upsilon(1S) \to J/\psi + X$ simulation and that obtained using the $B \to J/\psi + X$ simulation. This results in additional contributions of 4% for $J/\psi \to \mu^+\mu^-$ and 6% for $J/\psi \to e^+e^-$. We also include an additional 5% uncertainty in each due to limited MC statistics. We therefore estimate 9% systematic uncertainty in the $J/\psi \to \mu^+\mu^-$ reconstruction efficiency and 8% for $J/\psi \to e^+e^-$.

The uncertainty in the signal yield is estimated by floating the Gaussian widths used in fitting each x bin. We find that the signal yield changes by 3% for both the $J/\psi \to \mu^+\mu^-$ and $J/\psi \to e^+e^-$ analyses. The systematic error due to uncertainty in the shape of the background was estimated by comparing a linear background shape with an exponential. The difference is found to be 2% for $J/\psi \to \mu^+\mu^-$ and 1% for $J/\psi \to e^+e^-$.

Systematic uncertainty in the background subtraction comes from lack of precise knowledge of the continuum cross section ($e^+e^- \to J/\psi + X$) and the error in the extrapolation from the $\Upsilon(4S)$ energy to the $\Upsilon(1S)$ energy. The latter includes uncertainties in the ratio of luminosities and the branching fraction $\mathcal{B}(\Upsilon(1S) \to \mu^+\mu^-)$. Our measurement of the rate for $e^+e^- \to J/\psi + X$ is uncertain at the level of 10% (statistical uncertainty only) and the extrapolation factor of 1.41 ± 0.18 is uncertain at the level of 13%. We therefore estimate that the overall background rate is uncertain at the level of 16%. This uncertainty is propagated to an error in the branching fraction by shifting the central value for the background (see Fig. 8) up and then down by 1 standard deviation, and in each case, computing the change in the branching fraction from the nominal value. The corresponding shift in the branching fraction for $\Upsilon(1S) \to J/\psi + X$ is found to be 6% for both $J/\psi \to \mu^+\mu^-$ and $J/\psi \to e^+e^-$, which is taken as the systematic uncertainty due to the background subtraction. The uncertainty on the background subtraction does not have a significant effect on the general shape of the momentum distribution since its contribution is only about 10% of the total.

We also include the uncertainty in the number of $\Upsilon(1S)$ decays, which is estimated to be 1% based on the number of $\Upsilon(1S)$ events and the uncertainty in the off-to-on $\Upsilon(1S)$ luminosity ratio. We also include a 2% relative uncertainty in $\mathcal{B}(J/\psi \to l^+l^-)$. The total uncertainty is therefore found to be 12% for the $J/\psi \to \mu^+\mu^-$ channel and 11% for $J/\psi \to e^+e^-$ channel.

The systematics are itemized and shown in columns two and three in Table III.

B. Uncertainties in $\Upsilon(1S) \to \psi(2S) + X$ analysis

For the $\psi(2S)$ (as well as the χ_{cJ}) analysis, many of the systematic uncertainties cancel since these measurements are reported as a ratio with respect to the $\Upsilon(1S) \to J/\psi + X$ branching fraction. The uncertainty in the $\psi(2S)$ reconstruction efficiency comes from limited MC statistics (5%) and an imperfect understanding of $\Upsilon(1S) \to \psi(2S) + X$ events. The uncertainty from the latter is taken to be half the difference between the efficiency obtained using our default $\Upsilon(1S) \to \psi(2S) + X$ simulation and the $B \to \psi(2S) + X$ simulation. The two simulations agree to within 1% in absolute value, which translates into an additional 5% relative systematic uncertainty in the reconstruction efficiency for each channel. We also include a systematic uncertainty of 1% per track for each of the two pions in the decay $\psi(2S) \to J/\psi\pi^+\pi^-$ (2%). We therefore estimate that the noncanceling systematic uncertainty in the $\psi(2S)$ reconstruction efficiency is 7%.

Uncertainty in the signal yield is estimated by shifting the Gaussian width up and down by 20% about the central value (2.5 MeV/c^2) and taking half of the average deviation, which results in a 7% systematic uncertainty.

TABLE III. Sources of systematic uncertainty in the $\Upsilon(1S) \to J/\psi + X$, $\Upsilon(1S) \to \psi(2S) + X$, and $\Upsilon(1S) \to \chi_{cJ} + X$ analyses.

Source	Value (%)					
	$J/\psi \to \mu^+\mu^-$	$J/\psi \to e^+e^-$	$\psi(2S)$	χ_{c0}	χ_{c1}	χ_{c2}
Reconstruction efficiency	9%	8%	7%	12%	12%	12%
Signal yield	3%	3%	7%	···	6	1
Background shape	2%	1%	6%	···	6	6
Background subtraction	6%	6%	15%	···	···	···
No. of $\Upsilon(1S)$ decays	1%	1%	···	···	···	···
Error in $\mathcal{B}(J/\psi \to l^+l^-)$	2%	2%	···	···	···	···
Error in $\mathcal{B}[\psi(2S) \to \psi\pi^+\pi^-]$	···	···	5%	···	···	···
Error in $\mathcal{B}(\chi_{c0,1,2} \to J/\psi\gamma)$	···	···	···	20%	10%	11%
Total	12%	11%	20%	25%	18%	17%

Uncertainty in signal yield due to the assumed background shape was estimated by fitting the background to the alternate functional form: $A(1 - B\exp(-Cx))$ (the default is a second-order polynomial). The yield differs by 6%, which is taken as the associated uncertainty.

Uncertainty due to the background subtraction is estimated by considering a $\pm 50\%$ change in the expected background contribution, which is about 2 standard deviations. The resulting systematic uncertainty in the branching ratio is 15%. Uncertainty in the branching fraction $\mathcal{B}(\psi(2S) \to \psi\pi^+\pi^-)$ contributes 5%. We therefore estimate a total systematic uncertainty of 20% in the $\psi(2S)$ branching fraction ratio.

C. Uncertainties in $\Upsilon(1S) \to \chi_{cJ} + X$ analyses

The uncertainty in the efficiencies for reconstructing $\chi_{cJ} \to J/\psi\gamma$ is taken to be half the difference in the efficiencies for reconstructing χ_{cJ} in B decays at the $\Upsilon(4S)$ versus in $\Upsilon(1S)$ decays (8%). We include an additional uncertainty of 8% to reflect the lower value we obtain for $\mathcal{B}(B \to \chi_{c1} + X)$ as compared to the world average. This also accounts for any possible systematic uncertainty in the photon reconstruction efficiency. We attribute a 3% uncertainty for each due to limited MC statistics. We therefore estimate an overall systematic uncertainty in the reconstruction efficiency of the $\chi_{cJ} + X$ final state of 12%.

The uncertainty in the signal yield is obtained by allowing the Gaussian widths to float, from which we obtain differences of 6% and 1% for the $J = 1$ and $J = 2$ states. The uncertainty from the background determination is estimated by using different ranges over which to fit the background. We find maximum variations of 12%, of which we take half as the associated systematic uncertainty (6%). Since there is no evidence of any χ_{cJ} signal in the continuum, we do not consider this as a source of systematic uncertainty. Lastly, we include uncertainties in the $\chi_{cJ} \to J/\psi\gamma$ branching fractions [22] of 20%, 10%, and 11% for $J = 0$, 1, and 2 states, respectively. We therefore estimate total systematic uncertainties of 18% for χ_{c1} and 17% for χ_{c2}. The uncertainty on the limits for χ_{c0} are estimated to be 25%, and the upper limits are increased by this amount to reflect this systematic uncertainty.

Systematics uncertainties are listed and summarized in Table III.

VII. SUMMARY

We present vastly improved measurements of the rates for production of charmonium in $\Upsilon(1S)$ decays over previous measurements. We have measured both the branching fraction for $\Upsilon(1S) \to J/\psi + X$ and the scaled momentum distribution, as well as distributions in the polar angle and helicity in $\Upsilon(1S)$ decay. We also report on first observations of the decays $\Upsilon(1S) \to \psi(2S) + X$ and evidence for $\Upsilon(1S) \to \chi_{c1,2} + X$.

The branching fractions for $\Upsilon(1S) \to J/\psi + X$ are measured in both the $J/\psi \to \mu^+\mu^-$ and $J/\psi \to e^+e^-$ channels. Their branching fractions, $\mathcal{B}(\Upsilon(1S) \to J/\psi + X)$ are measured to be $[6.9 \pm 0.5(\text{stat}) \pm 0.8(\text{syst})] \times 10^{-4}$ and $[6.1 \pm 0.5(\text{stat}) \pm 0.7(\text{syst})] \times 10^{-4}$, respectively. The two are averaged to obtain

$$\mathcal{B}(\Upsilon(1S) \to J/\psi + X) = (6.4 \pm 0.4(\text{stat}) \pm 0.6(\text{syst})) \times 10^{-4}. \quad (9)$$

We also measure the branching fraction $\mathcal{B}(\Upsilon(1S) \to \psi(2S) + X)$ relative to $\mathcal{B}(\Upsilon(1S) \to J/\psi + X)$, and find

$$\frac{\mathcal{B}(\Upsilon(1S) \to \psi(2S) + X)}{\mathcal{B}(\Upsilon(1S) \to J/\psi + X)} = 0.41 \pm 0.11(\text{stat}) \pm 0.08(\text{syst}). \quad (10)$$

This report also presents the first evidence of the decay $\Upsilon(1S) \to \chi_{cJ} + X$. The branching fractions for all measured modes are summarized in Table IV.

The $\Upsilon(1S) \to J/\psi + X$ branching fraction is consistent with predictions of both the color-octet mechanism for J/ψ production in $\Upsilon(1S)$ decays [15,16] and color-singlet production via $\Upsilon(1S) \to J/\psi c\bar{c}g + X$ [13], each which predict a branching fraction at the level of 6×10^{-4}. The observed scaled momentum spectrum is relatively soft, peaking around $x \simeq 0.3$, in contrast to J/ψ's produced in the continuum, which peak at about 0.7. The peaking at low momentum is in sharp contrast to the prediction of the color-octet model which predicts a peaking of x near 1. It is possible that incorporation of final state interactions could improve this agreement as was shown for $e^+e^- \to J/\psi + X$ [11]. The observed spectrum is closer to, although softer than, the expectation of the color-singlet process [13], $\Upsilon(1S) \to J/\psi c\bar{c}g + X$, which peaks near $x \simeq 0.5$. When this parton-level calculation is simulated using PYTHIA we are able to achieve satisfactory agreement in the region $x < 0.6$ when hadronization of the recoiling charm quarks into charm hadrons is included, and our measured feed-downs of $\psi(2S)$ and χ_{cJ} to J/ψ are incorporated.

The observation of $\Upsilon(1S) \to \psi(2S) + X$ is the first to a $c\bar{c}$ final state other than J/ψ. The feed-down to J/ψ constitutes $(24 \pm 6 \pm 5)\%$ of the inclusive rate for $\Upsilon(1S) \to J/\psi + X$, which is significantly larger than expected in either the color-octet [15] or color-singlet model [13], each which predict a feed-down to J/ψ at the level of 10%. Our measured rates for $\Upsilon(1S) \to \chi_{cJ} + X$ yield feed-down contributions of $(11 \pm 3 \pm 2)\%$ for the $J = 1$ state and $(10 \pm 2 \pm 2)\%$ for the $J = 2$ state, which is also larger than the expected contribution of about 10%, summed over $J = 0$, 1, and 2 [13,15,17].

These measurements can shed additional light on the role of the color-octet and color-singlet mechanisms in producing charmonium, not only in $\Upsilon(1S)$ decays but also

TABLE IV. Summary of measurements of the branching fractions for $\Upsilon(1S)$ to charmonium final states. The $\psi(2S)$ and χ_{cJ} branching fractions are expressed relative to $\mathcal{B}(\Upsilon(1S) \to J/\psi + X)$. The last column shows the feed-down contributions to $\Upsilon(1S) \to J/\psi + X$. For the χ_{c0} we show upper limits at 90% confidence level. Where uncertainties are shown, the first is statistical and the second is systematic.

Final state, f	$\mathcal{B}(\Upsilon(1S) \to f + X)$	
J/ψ	$(6.4 \pm 0.4 \pm 0.6) \times 10^{-4}$	
	$\mathcal{B}(\Upsilon(1S) \to f + X)/\mathcal{B}(\Upsilon(1S) \to J/\psi + X)$	Feed-down to J/ψ
$\psi(2S)$	$0.41 \pm 0.11 \pm 0.08$	$0.24 \pm 0.06 \pm 0.05$
χ_{c0}	<7.4	<0.082
χ_{c1}	$0.35 \pm 0.08 \pm 0.06$	$0.11 \pm 0.03 \pm 0.02$
χ_{c2}	$0.52 \pm 0.12 \pm 0.09$	$0.10 \pm 0.02 \pm 0.02$

in e^+e^- and $p\bar{p}$ collisions. In this regard, it would be of great interest to determine whether the same softening mechanism applied to the color-octet prediction for $e^+e^- \to J/\psi + X$ [11] can account for the J/ψ momentum spectrum in $\Upsilon(1S) \to J/\psi + X$. Moreover, computation of the angular distributions for the color-octet and color-singlet mechanisms may provide additional discrimination between these two processes. From an experimental perspective, the additional information on the roles of color-singlet versus color-octet mechanisms may be obtained by measuring the ratio $\sigma(p\bar{p} \to J/\psi c\bar{c} + X)/\sigma(p\bar{p} \to J/\psi + X)$ at the Tevatron. The unexpectedly large value for $\sigma(e^+e^- \to J/\psi c\bar{c} + X)/\sigma(e^+e^- \to J/\psi + X)$ reported by Belle [14] may point to a large rate in $p\bar{p}$ collisions as well.

ACKNOWLEDGMENTS

We gratefully acknowledge the effort of the CESR staff in providing us with excellent luminosity and running conditions. This work was supported by the National Science Foundation and the U.S. Department of Energy. We also thank Kingman Cheung and Wai-Yee Keung for their assistance with the color-octet predictions and Shiyuan Li for providing color-singlet predictions.

[1] J. E. Augustin *et al.*, Phys. Rev. Lett. **33**, 1406 (1974).
[2] J. J. Aubert *et al.*, Phys. Rev. Lett. **33**, 1404 (1974).
[3] N. Cabibbo, Phys. Rev. Lett. **10**, 531 (1963); M. Kobayashi and K. Maskawa, Prog. Theor. Phys. **49**, 652 (1973).
[4] CDF Collaboration, F. Abe *et al.*, Phys. Rev. Lett. **69**, 3704 (1992); **71**, 2537 (1993); **75**, 1451 (1995).
[5] E. Braaten and S. Fleming, Phys. Rev. Lett. **74**, 3327 (1995).
[6] CDF Collaboration, T. Affolder *et al.*, Phys. Rev. Lett. **85**, 2886 (2000).
[7] M. Cacciari and M. Kramer, Phys. Rev. Lett. **76**, 4128 (1996), and references therein.
[8] E. Braaten and Y. Chen, Phys. Rev. Lett. **76**, 730 (1996).
[9] *BABAR* Collaboration, B. Aubert *et al.*, Phys. Rev. Lett. **87**, 162002 (2001).
[10] Belle Collaboration, K. Abe *et al.*, Phys. Rev. Lett. **88**, 052001 (2002).
[11] S. Fleming, A. Leibovich, and T. Mehen, Phys. Rev. D **68**, 094011 (2003).
[12] Z. H. Lin and G. Zhu, Phys. Lett. B **597**, 382 (2004).
[13] S. Li, Q. Xie, and Q. Wang, Phys. Lett. B **482**, 65 (2000).
[14] Belle Collaboration, K. Abe *et al.*, Phys. Rev. Lett. **89**, 142001 (2002).
[15] K. Cheung, W. Keung, and T. Yuan, Phys. Rev. D **54**, 929 (1996).
[16] M. Napsuciale, Phys. Rev. D **57**, 5711 (1998).
[17] H. Trottier, Phys. Lett. B **320**, 145 (1994).
[18] CLEO Collaboration, R. Fulton *et al.*, Phys. Lett. B **224**, 445 (1989).
[19] ARGUS Collaboration, H. Albrecht *et al.*, Z. Phys. C **55**, 25 (1992).
[20] CLEO Collaboration, S. Kopp *et al.*, Nucl. Instrum. Methods Phys. Res., Sect. A **384**, 61 (1996); CLEO Collaboration, A. Wolf *et al.*, Nucl. Instrum. Methods Phys. Res., Sect. A **408**, 58 (1998); CLEO Collaboration, G. Viehhauser *et al.*, Nucl. Instrum. Methods Phys. Res., Sect. A **462**, 146 (2001); CLEO Collaboration, Y. Kubota *et al.*, Nucl. Instrum. Methods Phys. Res., Sect. A **320**, 66 (1992).
[21] G. C. Fox and S. Wolfram, Phys. Rev. Lett. **41**, 1581 (1978).
[22] K. Hagiwara *et al.*, Phys. Rev. D **66**, 010001 (2002), and 2003 off-year partial update for the 2004 edition available on the PDG WWW page (URL: http://pdg.lbl.gov/).
[23] T. Sjöstrand *et al.*, Comput. Phys. Commun. **135**, 238 (2001).
[24] R. Brun *et al.*, CERN Report No. CERN-DD/EE84-1, 1987 (unpublished).

[25] CLEO Collaboration, W. Y. Chen *et al.*, Phys. Rev. D **39**, 3528 (1989).
[26] R. Kleiss and S. van der Marck, Nucl. Phys. **B342**, 61 (1990).
[27] S. Baek, P. Cho, J. Lee, and H. S. Song, J. Korean Phys. Soc. **33**, 97 (1998).
[28] P. Cho and A. K. Leibovich, Phys. Rev. D **54**, 6690 (1996).
[29] D. J. Lange, Nucl. Instrum. Methods Phys. Res., Sect. A **462**, 152 (2001).
[30] M. Benayoun *et al.*, Mod. Phys. Lett. A **14**, 2605 (1999).
[31] *BABAR* Collaboration, B. Aubert *et al.*, Phys. Rev. D **67**, 032002 (2003); Belle Collaboration, K. Abe *et al.*, Phys. Rev. Lett. **89**, 011803 (2002); CLEO Collaboration, S. Chen *et al.*, Phys. Rev. D **63**, 031103 (2001).